Geophys. J. Int. (2000) **142,** 855–875

Observations of flexure and the rheology of oceanic lithosphere

A. B. Watts[1] and S. Zhong[2]

[1] *Department of Earth Sciences, Parks Road, Oxford* OX1 3PR, *UK. E-mail: tony@earth.ox.ac.uk*
[2] *Department of Earth, Atmospheric, and Planetary Sciences, Massachusetts Institute of Technology, Cambridge,* MA 02139–4307, *USA*

Accepted 2000 April 6. Received 2000 April 6; in original form 1999 September 3

SUMMARY

The principal evidence for the long-term (i.e. >1 Myr) mechanical behaviour of the oceanic lithosphere has come from studies of how it deforms in response to large loads such as volcanoes and sediments. A model widely used to explain the deformation is an elastic plate in which flexural rigidity depends on the thermal age of the lithosphere *at the time of loading*. An elastic model, however, is time-invariant and does not take into account temporal changes that may occur in the flexural rigidity as a consequence of loading. There is evidence, for example, that the flexural rigidity of the oceanic lithosphere also depends on load age, being large at short times and small at long times. Thus, competing effects may exist between thermal cooling which strengthens the lithosphere and some form of load-induced stress relaxation which weakens it.

In order to investigate the relative roles of these processes, we have developed a multilayered viscoelastic model which is based on the results of experimental rock mechanics that creep in the lithosphere is a thermally activated process, and on a thermal structure that is given by the plate-cooling model. By comparing the predictions of the model with a new compilation of flexural rigidity estimates, we have found that, if the upper mantle viscosity is 10^{20} Pa s, the activation energy that best describes the long-term mechanical behaviour of the oceanic lithosphere is 120 KJ mol^{-1}. This parameter pair explains the dependence of flexural rigidity on *both* plate and load age. It also helps account for the subsidence and uplift history of oceanic islands and the stratigraphic patterns that develop in the flexural moats that flank them. At atolls, a multilayered viscoelastic model explains the rapid subsidence that follows shield building and does not require that the age of the lithosphere that supports a volcano is thermally 're-set' to a younger value. Our studies suggest that, while the oceanic lithosphere has viscoelastic properties, the viscosity of its upper layers is so much higher than that of its lower layers that in effect it behaves as a thin elastic plate on long timescales. There will therefore be a certain permanence to the observations of oceanic flexure such that they may be used, with some confidence, to evaluate the tectonic setting of individual features of the seafloor and, in some cases, their age.

Key words: flexure of the lithosphere, isostasy, rheology.

1 INTRODUCTION

The rheology of the lithosphere is a topic that is currently of much interest in geodynamics. The way that the lithosphere responds to loads such as ice sheets, sediments and volcanoes has implications, for example, for understanding the subsidence and uplift history of the interior of the plates as well as the structural styles that develop at the plate boundaries. In addition, knowledge of the long-term mechanical properties of the lithosphere is important for our understanding of the surface expressions of processes, such as mantle convection, that occur below the lithosphere.

Data from experimental rock mechanics imply that the strength of rocks increases with depth and then decreases, as pressure and temperature increase. When this strength is exceeded, rocks deform in fundamentally different ways: in the relatively cool upper part of the crust, they deform by brittle deformation (e.g. Byerlee 1978), while in the relatively hot lower part of the crust and upper mantle they deform by ductile flow (e.g. Goetze 1978). Brittle deformation occurs by frictional sliding on small fractures in the rock. Ductile deformation, in contrast, occurs by some form of thermally activated creep mechanism.

One problem with laboratory-based studies is the short timescales that are involved. As a result, laboratory strain rates are

high (i.e. $10^{-4}-10^{-6}$ s^{-1}) when compared with those associated with geological processes in compressional (e.g. orogeny) and extensional (e.g. rift-type basin formation) settings which, typically, are in the range $10^{-15}-10^{-19}$ s^{-1} (e.g. Cloetingh & Burov 1996; Newman & White 1997). Although the general effect of strain rate on rock strength is known from laboratory studies, with rocks becoming weaker as the strain rate is decreased from 10^{-4} to 10^{-6} s^{-1}, the rheology of the crust and mantle at the much lower strain rates of geological processes is poorly understood.

Probably the best constraints on how the Earth deforms on longer timescales has come from studies of the way that it responds to the waxing and waning of ice sheet loads (e.g. Cathles 1975). During the Late Pleistocene, for example, large tracts of North America and northern Europe were covered by an ice sheet which depressed the crust and mantle beneath it and raised it in flanking regions. As climate changed, the locus of the ice sheet loads shifted, causing the crust and mantle to adjust. With each ice withdrawal, for example, the crust and mantle were unloaded, causing uplift where the loads once were and subsidence in flanking regions. By determining the rates of uplift and subsidence and comparing them with the predictions of spherical earth models composed of Newtonian fluid layers, it has been possible to use the pattern of rebound to constrain the viscosity structure of the mantle. Studies of Fennoscandia (Fjeldskaar 1994), Lake Bonneville (Iwasaki & Matsu'ura 1982) and North America (Wu & Peltier 1983) suggest, for example, a viscosity of $7\times10^{20}-1\times10^{21}$, $1–2\times10^{20}$ and 10^{21} Pa s, respectively, for the weak asthenospheric layer that underlies the lithosphere. More recently, Vermeersen *et al.* (1998) used new observations of the long-wavelength time-dependent gravity field perturbations that are driven by Pleistocene deglaciation to estimate that the viscosity of the mantle is $\ll10^{21}$ Pa s, and in the range 10^{20} to a few times 10^{20} Pa s.

While the pattern of glacial rebound provides most information on the asthenosphere, there is evidence that the lithosphere influences the pattern of deformation. In particular, McConnell (1968) showed that the Fennoscandia uplift data require an elastic lithosphere that extends to depths of 120 km. Furthermore, sea-level observations from central Sweden and southern Finland (Wolf 1987) suggest an elastic thickness of the lithosphere of 80 km. Similar values have been deduced from the pattern of rebound of raised shorelines that once stood as 'islands' in the pro-glacial lakes of North America (Walcott 1970c). Finally, Mitrovica & Peltier (1993) argued, using an inversion technique, that uplift data in Fennoscandia require an elastic lithosphere 70–145 km thick.

When compared with the timescales of geological processes such as rifting and orogeny, however, the timescales of glacial loading are still short. Information on the deformation of the lithosphere on these timescales has therefore come from volcanoes, sediments, and the loads that deform the oceanic lithosphere as it approaches an island-arc deep-sea trench system. Not only are these loads of long duration (>1 Ma), but they tend to be more concentrated than ice loads. As a result, they have provided information on the long-term mechanical properties of the lithosphere over relatively small spatial scales.

One of the most successful models that has been used (e.g. Gunn 1943) to describe the deformation of the lithosphere is the elastic plate model. In this model, the lithosphere is treated as a thin elastic plate that overlies an inviscid substratum. By comparing the predictions of the model with observations of flexure in the region of volcanoes and sediments, for example, it has been possible to constrain the long-term elastic properties of the lithosphere and their relationship to both plate and load age (e.g. Watts 1978; Caldwell & Turcotte 1979; Cazenave *et al.* 1980) in a wide range of tectonic settings.

Despite this success, the elastic model is time-invariant and does not take into account the possibility of changes in the flexural properties of the lithosphere with time. For example, we know from both oceanic and continental flexure studies that the long-term elastic thickness of the lithosphere is much less than the seismic thickness. Since seismic waves are of shorter duration than volcanic and other types of geological loads, these observations suggest a model in which the thickness of the lithosphere that mechanically supports a load is initially thick and then becomes thinner as time increases.

An example of such a model is a thin viscoelastic plate that overlies an inviscid substratum. Walcott (1970a) showed that this model could explain why young ice loads on the continental lithosphere were associated with high values of the elastic thickness while older volcanic loads on the oceanic lithosphere had lower values. Both the continental and oceanic data, in his view, could be explained by a relaxation time of 10^6 yr, which corresponds to a viscosity of the lithosphere of 10^{24} Pa s. The thin viscoelastic plate model therefore began to be quite widely applied. For example, Sleep & Snell (1976) and Quinlan & Beaumont (1984) used the model to explain the development of offlap patterns in sedimentary basins in North America, while Lambeck & Nakiboglu (1981) used it to account for the relationship between flexural rigidity and load age in the Society and Southern Cook islands in the south-central Pacific Ocean. Finally, a viscoelastic model was invoked in early continent-wide admittance studies by McNutt & Parker (1978) in an attempt to explain why old continents (e.g. Australia) were associated with low values of the elastic thickness.

A problem with the thin viscoelastic plate model is that it implies that, on very long timescales, the response of the lithosphere to loads approaches that of an Airy model. Several arguments can be advanced to refute this. First, the existence of gravity anomalies in the old, cold, cratonic interiors implies that stresses in the lithosphere are maintained for long periods of time. Second, it is known from the gravity and geoid anomalies that they cause (Watts 1978) that old volcanic loads on the oceanic lithosphere (e.g. Emperor seamounts) are supported by a flexure rather than an Airy-type isostatic model.

Courtney & Beaumont (1983) recognized that, while the lithosphere relaxes when it is loaded, it is, in effect, elastic on long timescales. Rather than use a thin elastic or viscoelastic plate model therefore, they used a multilayered viscoelastic model. Their model was based on the assumption that creep in mantle-type rocks is a thermally activated process and that the temperature structure of the oceanic lithosphere can be prescribed by its age. They showed that such a model could explain the range of elastic thickness estimates that were observed, as well as their dependence on the thermal structure of the lithosphere. By comparing predictions and observations, they determined the creep activation energy, E, and a basal viscosity of the lithosphere, $\eta_{\rm base}$, that could fit the observations.

The elastic thickness estimates used by Courtney & Beaumont (1983) were based on a compilation by Bodine *et al.* (1981) which included 25 estimates from mid-oceanic ridges, deep-sea trench–island arc systems, oceanic islands and seamounts, and river deltas. Since the Bodine *et al.* (1981) study, some 145

additional estimates of elastic thickness have been published. A few of these estimates (e.g. at deep-sea trench–island arc systems) are corrections to previous values, while others replace earlier estimates because they are based on more accurate topography, gravity and geoid anomaly data. The majority of the new estimates, however, are from geological features not included in the Bodine *et al.* (1981) compilation.

In this paper, we use a new compilation of elastic thickness estimates to re-examine the question of the long-term mechanical properties of the oceanic lithosphere. First, we compare the estimates with the predictions of the thin elastic and viscoelastic plate models and demonstrate that, while these models serve a useful purpose in parametrizing the observations of flexure, they do not adequately describe how the lithosphere actually responds to both short- and long-term loads. We then construct a multilayered viscoelastic model for the oceanic lithosphere similar to the one originally developed by Courtney & Beaumont (1983), the main difference being that a propagator matrix technique rather than a Green's function approach is used to solve the flexure equations. By comparing the new compilation of elastic thickness estimates with predictions of the multilayered viscoelastic models we determine the 'best-fit' parameters for the activation energy and a reference viscosity of the oceanic lithosphere. Finally, we examine the implications of the best-fit parameters for the subsidence and uplift history of active and drowned volcanic islands and the stratigraphy of their flanking moats.

2 ESTIMATES OF T_e

During the past two decades there has been a wealth of new data on the manner that the oceanic lithosphere responds to loads that are emplaced on its surface. By comparing the gravity and geoid anomalies, seismic reflection profiles of the top and base of the flexed oceanic crust, and seismic refraction evidence of the detailed velocity versus depth structure in the region of volcanic, sediment and other types of loads with the predictions of simple elastic models, it has been possible to constrain the long-term mechanical properties of the lithosphere.

A commonly used parameter in flexure studies is the elastic thickness of the lithosphere, T_e. The elastic thickness is a measure of the resistance of the lithosphere to deformation (i.e. the stiffness), and is determined from the flexural rigidity, D, by

$$D = ET_e^3/12(1-\sigma^2), \tag{1}$$

where E is Young's modulus and σ is Poisson's ratio.

Table 1 is a summary of oceanic T_e estimates. Some estimates are from the same bathymetric feature and represent attempts to improve on the accuracy of earlier values. For example, the first estimates at seamounts and oceanic islands in French Polynesia and the Canary Islands were based only on ETOPO5 'grids' of bathymetric data (e.g. Calmant 1987; Filmer & McNutt 1989). These estimates have subsequently been revised (Goodwillie & Watts 1993; Dañobeitia *et al.* 1994; Watts *et al.* 1997) using new shipboard data. Other estimates are corrections to earlier values. For example, early estimates at island arc–deep-sea trench systems (e.g. Caldwell *et al.* 1976) did not adequately correct for the effects of yielding in regions of high plate curvature (McNutt 1984).

We have therefore re-evaluated the oceanic T_e data set, selecting only those values at a particular feature that are based on the best data, and values that have had corrections applied to them. The resulting data set reduces to 139 estimates, which is approximately 80 per cent of the total number published. As Fig. 1 shows, however, the reduced data set is still spatially representative, being widely distributed over each of the world's main ocean basins.

Fig. 2 shows a plot of T_e against the difference in age between the age of the underlying seafloor and the age of the

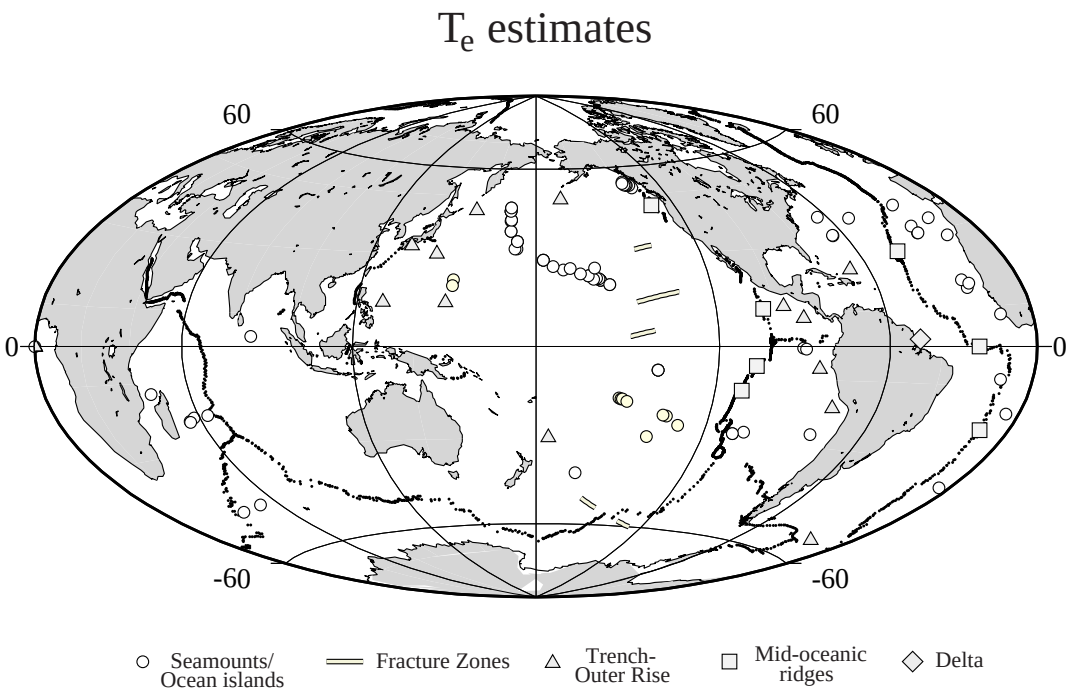

Figure 1. Locations of the T_e estimates (i.e. S, Sc, Spc, Tc, R and D in Table 1) used in this study.

Table 1. Summary of estimates of elastic thickness, T_e.

N	Type	Feature	Age of seafloor (Ma)	Seafloor age error (Myr)	Age of load (Ma)	Load age error (Myr)	T_e (km)	T_e error (km)	Reference
1	S	Hawaiian_Islands	80.0	1.5	1.5	1.5	28.2	0.0	(Walcott 1970b)
2	D	Amazon_Cone	100.0	12.5	7.5	2.5	31.1	10.0	(Cochran 1973)
3	S	Hawaii-Emperor	90.0	10.0	34.2	30.6	17.8	7.0	(Watts & Cochran 1974)
4	S	Great_Meteor	75.0	3.0	11.0	1.5	18.9	0.0	(Watts *et al.* 1975)
5	Tx	Kuril	107.5	3.0	0.0	0.0	20.0	2.5	(Caldwell *et al.* 1976)
6	Tx	Bonin	147.5	3.0	0.0	0.0	28.0	2.5	(Caldwell *et al.* 1976)
7	Tx	Mariana	155.0	3.0	0.0	0.0	29.0	2.5	(Caldwell *et al.* 1976)
8	Tx	Aleutian	57.5	3.0	0.0	0.0	28.0	2.5	(Caldwell *et al.* 1976)
9	R	Mid-Atlantic_Ridge	0.0	0.0	0.0	0.0	12.2	0.0	(McKenzie & Bowin 1976)
10	S	Hawaiian_Islands	80.0	3.0	2.5	2.5	24.1	4.0	(Suyenaga 1977)
11	Tx	Kuril	107.5	12.5	0.0	0.0	31.1	10.0	(McAdoo *et al.* 1978)
12	S	Hawaiian_Ridge	80.0	3.0	8.0	8.0	27.2	2.5	(Watts 1978)
13	S	Emperor_Seamounts	80.0	3.0	55.0	10.0	15.0	2.5	(Watts 1978)
14	S	Oahu	80.0	3.0	3.0	1.0	30.0	2.0	(Watts 1978)
15	S	Oahu	80.0	3.0	3.0	1.0	32.0	2.0	(Watts 1978)
16	S	Kauai/Oahu	80.0	3.0	5.0	1.0	30.0	2.0	(Watts 1978)
17	S	Kaula	80.0	3.0	7.5	1.0	30.0	2.0	(Watts 1978)
18	S	Kaula	80.0	3.0	7.5	1.0	20.0	2.0	(Watts 1978)
19	S	Raita_Bank	96.0	3.0	13.0	1.0	17.5	2.0	(Watts 1978)
20	S	Midway	105.0	3.0	18.0	1.0	37.0	2.0	(Watts 1978)
21	S	Koku	115.0	3.0	44.0	1.0	30.5	2.0	(Watts 1978)
22	S	Koku	115.0	3.0	48.5	1.0	36.0	2.0	(Watts 1978)
23	S	Nin_Toku	80.0	3.0	52.0	1.0	20.0	2.0	(Watts 1978)
24	S	Jimmu	80.0	3.0	56.0	1.0	10.5	2.0	(Watts 1978)
25	S	Suiko	80.0	3.0	58.5	1.0	13.0	2.0	(Watts 1978)
26	Sp	Rarotonga	87.0	5.0	1.5	0.1	14.0	0.0	(McNutt & Menard 1978)
27	S	Reunion	58.0	1.0	0.0	0.0	17.0	3.0	(McNutt & Menard 1978)
28	Sp	Tahiti	79.0	0.5	0.8	0.1	14.0	0.0	(McNutt & Menard 1978)
29	R	East_Pacific_Rise	0.0	0.0	0.0	0.0	4.0	2.0	(Cochran 1979)
30	R	Mid-Atlantic_Ridge	0.0	0.0	0.0	0.0	10.0	3.0	(Cochran 1979)
31	R	Juan_de_Fuca_Ridge	0.0	0.0	0.0	0.0	4.0	1.0	(McNutt 1979)
32	S	Western_Walvis_Ridge	5.0	5.0	0.0	0.0	6.5	1.5	(Detrick & Watts 1979)
33	T	Nankai	22.0	3.0	0.0	0.0	15.0	1.5	(Caldwell & Turcotte 1979)
34	Tx	Middle_America	32.5	2.5	0.0	0.0	18.6	2.2	(Caldwell & Turcotte 1979)
35	Tx	Aleutian	60.0	10.0	0.0	0.0	39.6	15.0	(Caldwell & Turcotte 1979)
36	S	Crozet	80.0	2.5	5.0	0.5	22.5	0.0	(Cazenave *et al.* 1980)
37	S	Marquesas	42.5	2.5	2.5	X	16.5	2.0	(Cazenave *et al.* 1980)
38	Sp	Society	70.0	0.0	2.2	X	20.9	2.0	(Cazenave *et al.* 1980)
39	Sp	Rarotonga	82.2	0.9	1.5	X	11.5	1.5	(Lambeck 1981b)
40	Sp	Society_Tahiti	69.0	5.0	2.2	X	15.0	1.5	(Lambeck 1981a)
41	S	Ojin	80.0	15.0	51.0	2.5	10.0	1.5	(Watts & Ribe 1984)
42	S	Suiko	80.0	15.0	55.3	2.5	17.0	2.5	(Watts & Ribe 1984)
43	Tc	Middle_America	20.0	5.0	0.0	0.0	17.5	2.5	(McNutt 1984)
44	T	Peru	30.0	5.0	0.0	0.0	22.5	2.5	(McNutt 1984)
45	T	Chile	41.0	5.0	0.0	0.0	27.0	2.5	(McNutt 1984)
46	T	Kermadec	100.0	10.0	0.0	0.0	40.7	0.7	(McNutt 1984)
47	Tc	Aleutian	55.0	5.0	0.0	0.0	33.0	2.0	(McNutt 1984)
48	Tc	Kuril	105.0	5.0	0.0	0.0	42.5	12.5	(McNutt 1984)
49	Tc	Bonin	130.0	5.0	0.0	0.0	39.0	6.0	(McNutt 1984)
50	Tc	Mariana	148.0	5.0	0.0	0.0	40.0	5.0	(McNutt 1984)
51	R	East_Pacific_Rise	0.0	0.0	0.0	0.0	0.7	0.7	(Madsen *et al.* 1984)
52	S	Louisville,_Valerie	85.0	11.0	35.0	2.0	18.0	1.5	(Cazenave & Dominh 1984)
53	T	Middle_America	20.0	5.0	0.0	0.0	29.7	5.0	(McAdoo & Martin 1984)
54	T	Phillipine	110.0	10.0	0.0	0.0	26.8	5.0	(McAdoo & Martin 1984)
55	T	Bonin	130.0	5.0	0.0	0.0	63.0	5.0	(McAdoo & Martin 1984)
56	T	Mariana	148.0	5.0	0.0	0.0	51.3	5.0	(McAdoo & Martin 1984)

Table 1. (*Continued.*)

N	Type	Feature	Age of seafloor (Ma)	Seafloor age error (Myr)	Age of load (Ma)	Load age error (Myr)	T_e (km)	T_e error (km)	Reference
57	T	Aleutian	55.0	5.0	0.0	0.0	35.4	5.0	(McAdoo & Martin 1984)
58	T	Kuril	105.0	5.0	0.0	0.0	41.9	5.0	(McAdoo & Martin 1984)
59	T	South_Sandwich	75.0	10.0	0.0	0.0	56.3	5.1	(McAdoo *et al.* 1985)
60	T	Peru	37.5	2.5	0.0	0.0	42.7	4.3	(McAdoo *et al.* 1985)
61	T	Puerto_Rico	80.0	5.0	0.0	0.0	31.7	5.2	(McAdoo *et al.* 1985)
62	R	Mid_Atlantic_Ridge	0.0	0.0	0.0	0.0	8.0	1.0	(Bowin & Milligan 1985)
63	S	Marquesas	80.0	5.0	60.0	5.0	20.0	5.0	(Fischer *et al.* 1986)
64	R	East_Pacific_Rise	0.0	0.0	0.0	0.0	0.1	0.1	(Kuo & Parmentier 1986)
65	Spx	McDonald	43.0	2.0	0.0	0.0	2.0	2.0	(Calmant & Cazenave 1986)
66	Sp	Rapa	52.0	5.0	5.1	0.1	2.0	2.0	(Calmant & Cazenave 1986)
67	Sp	Raivavae	65.0	5.0	6.4	1.0	9.0	1.0	(Calmant & Cazenave 1986)
68	Sp	Tubuai	70.0	5.0	9.5	0.9	8.0	0.5	(Calmant & Cazenave 1986)
69	Sp	Rimatora	78.0	5.0	13.5	0.0	10.0	1.0	(Calmant & Cazenave 1986)
70	Spx	Maria	80.0	5.0	15.0	0.0	10.0	0.5	(Calmant & Cazenave 1986)
71	Sp	Mangaia	85.0	5.0	17.7	0.8	7.0	1.0	(Calmant & Cazenave 1986)
72	Sp	Atiu	87.0	5.0	4.0	0.0	9.5	0.5	(Calmant & Cazenave 1986)
73	Sp	Mauke	85.0	5.0	5.0	0.0	11.0	0.5	(Calmant & Cazenave 1986)
74	Sp	Aitutaki	87.0	5.0	7.0	0.0	10.0	1.0	(Calmant & Cazenave 1986)
75	Sp	Rarotonga	87.0	5.0	1.5	0.3	14.0	1.5	(Calmant & Cazenave 1986)
76	Spx	Tahiti	70.0	5.0	0.8	0.2	20.0	2.0	(Calmant & Cazenave 1986)
77	Sp	Bora-Bora	75.0	5.0	3.2	0.1	15.0	1.5	(Calmant & Cazenave 1986)
78	Spx	Maupiti	76.5	5.0	4.2	0.2	13.0	1.0	(Calmant & Cazenave 1986)
79	S	Marquesas	63.0	5.0	3.0	0.0	14.0	2.0	(Calmant 1987)
80	Spx	Gambier	29.5	2.0	6.3	0.0	6.0	0.1	(Calmant 1987)
81	Sp	Mururoa	35.0	2.0	7.0	0.0	6.0	2.0	(Calmant 1987)
82	S	Easter	4.3	0.5	0.3	0.0	3.0	3.0	(Calmant 1987)
83	S	Sala_y_Gomez	5.8	0.5	1.7	0.0	3.0	3.0	(Calmant 1987)
84	S	Kauai	93.5	0.0	5.0	0.0	32.5	1.5	(Calmant 1987)
85	S	Niihau	94.5	0.0	6.5	0.0	28.0	2.5	(Calmant 1987)
86	S	Nihoa	97.0	0.0	7.5	0.0	21.5	1.5	(Calmant 1987)
87	S	Necker	100.0	0.0	10.5	0.0	26.0	2.5	(Calmant 1987)
88	S	Raita_bank	108.0	0.0	17.0	0.0	21.0	1.5	(Calmant & Cazenave 1986)
89	S	Gardner_Pinnacles	106.0	0.0	15.0	0.0	25.5	1.2	(Calmant 1987)
90	S	Lisianski	114.0	0.0	22.0	0.0	25.5	3.0	(Calmant 1987)
91	S	Pearl_Hermes	116.5	0.0	20.5	0.0	27.0	2.5	(Calmant 1987)
92	S	Midway	119.0	0.0	27.0	0.0	26.5	2.5	(Calmant 1987)
93	S	Kanmu	121.0	0.0	40.0	0.0	20.0	2.0	(Calmant 1987)
94	S	Diakakuji	123.0	0.0	41.0	0.0	25.5	6.0	(Calmant 1987)
95	S	Koko	118.0	0.0	46.5	0.0	19.0	1.0	(Calmant 1987)
96	S	Ojin	118.0	0.0	55.0	0.0	19.0	2.0	(Calmant 1987)
97	S	Nintoku	110.0	0.0	56.0	0.0	22.5	3.5	(Calmant 1987)
98	S	Suiko	117.0	0.0	64.5	0.0	18.0	1.5	(Calmant 1987)
99	S	Jimmu	113.0	0.0	65.0	0.0	20.0	2.0	(Calmant 1987)
100	S	Cape_Verde	144.0	1.0	14.0	5.0	28.0	4.0	(McNutt 1988)
101	Sx	Hawaiian_Ridge	80.0	5.0	2.5	1.2	40.0	2.5	(Watts & 10 Brink 1989)
102	S	Bermuda	115.0	7.0	38.0	5.0	30.0	5.0	(Sheehan & McNutt 1989)
103	Spm	Magellans_Himu	163.0	0.6	119.6	0.6	10.0	2.0	(Smith *et al.* 1989)
104	Spm	Magellans_Hemler	163.0	0.5	100.1	0.5	15.0	3.0	(Smith *et al.* 1989)
105	Sx	Canary_Islands	155.0	7.5	10.0	3.0	48.0	3.0	(Filmer & McNutt 1989)
106	S	Afganasy-Nikitin	77.0	10.0	77.0	0.0	5.0	2.5	(Karner & Weissel 1990)
107	C	Indian_ocean_def	77.0	10.0	7.0	0.0	12.5	2.5	(Karner & Weissel 1990)
108	S	Atlantis	170.0	2.5	95.0	0.0	22.5	2.5	(Calmant *et al.* 1990)
109	S	Azores	32.0	2.5	30.0	0.0	3.0	3.0	(Calmant *et al.* 1990)
110	S	Corner	98.0	2.5	73.0	0.0	6.0	1.0	(Calmant *et al.* 1990)
111	S	Madeira	129.0	2.5	1.0	0.0	32.5	2.0	(Calmant *et al.* 1990)
112	S	Bermuda	117.0	2.5	30.0	0.0	32.5	8.0	(Calmant *et al.* 1990)

Table 1. (*Continued.*)

N	Type	Feature	Age of seafloor (Ma)	Seafloor age error (Myr)	Age of load (Ma)	Load age error (Myr)	T_e (km)	T_e error (km)	Reference
113	S	Cruiser	70.0	2.5	60.0	0.0	7.0	1.0	(Calmant *et al.* 1990)
114	S	Great_Meteor	80.0	2.5	14.0	0.0	19.0	2.0	(Calmant *et al.* 1990)
115	S	Cape_Verde	116.0	2.5	10.0	0.0	21.0	2.0	(Calmant *et al.* 1990)
116	S	Cape_Verde	140.0	2.5	10.0	0.0	30.0	5.0	(Calmant *et al.* 1990)
117	S	Ascension	7.0	2.5	2.0	0.0	7.0	1.0	(Calmant *et al.* 1990)
118	S	St_Helena	41.0	2.5	16.0	0.0	9.5	1.0	(Calmant *et al.* 1990)
119	S	Mayotte	150.0	2.5	5.0	0.0	40.5	4.0	(Calmant *et al.* 1990)
120	S	Rodriguez	10.5	2.5	1.5	0.0	3.0	3.0	(Calmant *et al.* 1990)
121	S	Mauritius	59.0	2.5	8.0	0.0	16.5	1.5	(Calmant *et al.* 1990)
122	S	Reunion	64.0	2.5	2.0	0.0	32.0	5.0	(Calmant *et al.* 1990)
123	S	P._Edward	39.0	0.0	0.0	0.0	16.5	3.0	(Calmant *et al.* 1990)
124	F	Clarion	78.0	6.0	0.0	0.0	37.9	0.0	(Wessel & Haxby 1990)
125	F	Clarion	73.0	6.0	0.0	0.0	35.8	0.0	(Wessel & Haxby 1990)
126	F	Clarion	66.0	5.0	0.0	0.0	42.0	0.0	(Wessel & Haxby 1990)
127	F	Clarion	53.0	5.0	0.0	0.0	37.8	0.0	(Wessel & Haxby 1990)
128	F	Clarion	49.0	5.0	0.0	0.0	30.4	0.0	(Wessel & Haxby 1990)
129	F	Clarion	45.0	4.0	0.0	0.0	29.3	0.0	(Wessel & Haxby 1990)
130	F	Clarion	38.0	3.0	0.0	0.0	27.0	0.0	(Wessel & Haxby 1990)
131	F	Clipperton	77.0	8.0	0.0	0.0	37.7	0.0	(Wessel & Haxby 1990)
132	F	Clipperton	56.0	5.0	0.0	0.0	32.4	0.0	(Wessel & Haxby 1990)
133	F	Murray	68.0	5.0	0.0	0.0	35.6	0.0	(Wessel & Haxby 1990)
134	F	Murray	65.0	5.0	0.0	0.0	34.7	0.0	(Wessel & Haxby 1990)
135	F	Murray	62.0	5.0	0.0	0.0	34.0	0.0	(Wessel & Haxby 1990)
136	F	Murray	53.0	5.0	0.0	0.0	31.6	0.0	(Wessel & Haxby 1990)
137	F	Udintsev	43.0	5.0	0.0	0.0	34.2	0.0	(Wessel & Haxby 1990)
138	F	Udintsev	17.0	5.0	0.0	0.0	22.4	0.0	(Wessel & Haxby 1990)
139	F	Udintsev	62.0	5.0	0.0	0.0	40.6	0.0	(Wessel & Haxby 1990)
140	F	Udintsev	34.0	5.0	0.0	0.0	30.6	0.0	(Wessel & Haxby 1990)
141	T	North_Peru	30.0	0.0	0.0	0.0	35.0	5.0	(Judge & McNutt 1991)
142	T	South_Peru	42.0	0.0	0.0	0.0	43.0	3.0	(Judge & McNutt 1991)
143	T	North_Chile	45.0	3.0	0.0	0.0	33.4	3.0	(Judge & McNutt 1991)
144	R	East_Pacific_Rise	0.0	0.0	0.0	0.0	0.4	0.1	(Wang & Cochran 1993)
145	Spc	McDonald	42.0	5.0	0.0	0.0	2.0	2.0	(Goodwillie & Watts 1993)
146	Spc	Pitcairn	23.0	5.0	5.9	0.0	2.0	2.0	(Goodwillie & Watts 1993)
147	Spc	Gambier	30.5	5.0	0.7	0.0	18.0	7.0	(Goodwillie & Watts 1993)
148	Spc	Maria	80.0	5.0	15.4	0.0	5.5	2.0	(Goodwillie & Watts 1993)
149	Spc	Maupiti	76.5	5.0	4.3	0.0	5.5	2.0	(Goodwillie & Watts 1993)
150	Spc	Raiatea	74.5	5.0	2.7	0.2	10.5	1.5	(Goodwillie & Watts 1993)
151	Spc	Huahine	74.0	5.0	2.3	0.0	12.0	5.0	(Goodwillie & Watts 1993)
152	Spc	Tahiti	70.0	5.0	0.8	0.0	23.5	1.5	(Goodwillie & Watts 1993)
153	Sc	Hawaiian_ridge	80.0	2.0	4.0	1.5	40.0	1.0	(Wessel 1993)
154	Sc	Oshawa	12.0	1.0	X	X	6.0	1.0	(Harris & Chapman 1994)
155	Sc	Graham	13.5	1.0	X	X	4.0	1.0	(Harris & Chapman 1994)
156	Sc	Bowie	16.4	1.0	1.0	0.5	18.0	1.0	(Harris & Chapman 1994)
157	Sc	Hodgkins	17.4	1.0	14.3	0.5	6.0	1.0	(Harris & Chapman 1994)
158	Sc	Davidson	18.5	1.0	17.4	0.5	5.0	1.0	(Harris & Chapman 1994)
159	Sc	Dickens	19.6	1.0	4.0	0.5	18.0	1.0	(Harris & Chapman 1994)
160	Sc	Denson	19.6	1.0	18.2	0.5	6.0	1.0	(Harris & Chapman 1994)
161	Tc	Queen_Charlotte_1	9.0	1.0	2.0	0.5	11.0	1.0	(Harris & Chapman 1994)
162	Tc	Queen_Charlotte_2	10.0	1.0	2.0	0.5	12.0	1.0	(Harris & Chapman 1994)
163	Tc	Queen_Charlotte_3	14.0	1.0	2.0	0.5	14.0	1.0	(Harris & Chapman 1994)
164	Tc	Queen_Charlotte_4	15.0	1.0	2.0	0.5	14.0	1.0	(Harris & Chapman 1994)
165	Tc	Queen_Charlotte_5	16.0	1.0	2.0	0.5	16.0	1.0	(Harris & Chapman 1994)
166	Tc	Queen_Charlotte_6	17.0	1.0	2.0	0.5	17.0	1.0	(Harris & Chapman 1994)
167	Tc	Queen_Charlotte_7	19.0	1.0	2.0	0.5	19.0	1.0	(Harris & Chapman 1994)
168	Sc	Canary_Islands	155.0	7.5	8.0	5.0	20.0	5.0	(Watts 1994)

Table 1. (*Continued.*)

N	Type	Feature	Age of seafloor (Ma)	Seafloor age error (Myr)	Age of load (Ma)	Load age error (Myr)	T_e (km)	T_e error (km)	Reference
169	Sc	Canary_Islands	150.0	5.0	20.0	2.5	35.0	5.0	(Dañobeitia & Canales 1994)
170	S	Galápagos	7.5	1.0	0.0	0.0	12.0	2.0	(Feighner & Richards 1994)
171	S	Galápagos	7.5	1.0	0.0	0.0	3.0	3.0	(Feighner & Richards 1994)
172	Tc	Aleutian	56.8	5.0	0.0	0.0	42.2	6.0	(Levitt & Sandwell 1995)
173	Tc	Antilles	101.6	12.0	0.0	0.0	40.7	5.0	(Levitt & Sandwell 1995)
174	Tc	Bonin	141.7	2.0	0.0	0.0	51.9	15.0	(Levitt & Sandwell 1995)
175	Tc	Chile	38.0	2.0	0.0	0.0	31.4	3.0	(Levitt & Sandwell 1995)
176	Tc	Japan	132.3	3.5	0.0	0.0	68.3	5.0	(Levitt & Sandwell 1995)
177	Tc	Java	93.1	1.0	0.0	0.0	37.1	8.0	(Levitt & Sandwell 1995)
178	Tc	Kuril	119.4	3.0	0.0	0.0	61.7	15.0	(Levitt & Sandwell 1995)
179	Tc	Mariana	143.6	1.0	0.0	0.0	46.7	10.0	(Levitt & Sandwell 1995)
180	Tc	Middle_America	19.9	8.0	0.0	0.0	27.3	10.0	(Levitt & Sandwell 1995)
181	Tc	Peru	34.8	5.0	0.0	0.0	44.7	14.0	(Levitt & Sandwell 1995)
182	Tc	Phillipine	117.9	0.0	0.0	0.0	62.0	0.0	(Levitt & Sandwell 1995)
183	S	Tuamotu	67.5	3.5	52.5	2.5	5.0	5.0	(Ito *et al.* 1995)
184	S	Easter_East	5.0	5.0	0.0	0.0	5.9	1.9	(Kruse *et al.* 1997)
185	S	San_Felix_island	30.8	2.0	0.8	0.0	10.6	2.9	(Kruse *et al.* 1997)
186	S	Ascension	7.0	1.0	0.9	0.3	3.0	0.5	(Minshull & Brozena 1997)

S = seamount/oceanic island: Sp = seamount/oceanic island in French Polynesia region; Spm = seamounts that 'backtrack' to French Polynesia region (e.g. Magellan seamounts). T = deep-sea trench–outer rise system. D = river delta. R = mid-oceanic ridge. F = fracture zone.
x = an old value, subsequently replaced by a corrected value. These values have not been plotted in Figs 2, 3, 5 and 10. c = corrected value (e.g. for curvature, swell bathymetry).

load. The plot confirms the simple relationship, first proposed by Watts (1978) based on a much smaller data set, between oceanic T_e and the age of the lithosphere *at the time of loading*. Features that formed on or near a ridge (e.g. Emperor seamounts) have a lower T_e than features that formed off-ridge (e.g. Hawaiian Islands). The new compilation shows that approximately 72 per cent of the T_e estimates fall within the depth to the 300–600 °C oceanic isotherms based on a cooling plate model. The main exceptions are estimates from fracture zones (and some island arc–deep-sea trench systems), where T_e appears to be systematically higher, and at some seamounts and oceanic islands in the French Polynesia region, where T_e seems to be lower.

An important result shown in Fig. 2 is that T_e is less than the seismic thickness of oceanic lithosphere, as inferred from surface-wave studies. If we use, for example, the two estimates of Nishimura & Forsyth (1989) which have been corrected for anisotropy, one for young (0–5 Ma) oceanic crust and the other for old (80–160 Ma) crust, then T_e is some 25–50 per cent less than the seismic thickness, with most values about 40 per cent less. Allowing for the time that it takes to build the submarine edifice of an oceanic volcano, the T_e estimates in Fig. 2 represent loads that are 1–2 Ma or older. In contrast, the seismic estimates are based on loads that are of the duration of a few seconds to a few hundred seconds. This suggests that, on loading, the thickness of the lithosphere that mechanically supports a load must decrease from its short-term seismic to its long-term elastic thickness. The timescale over which this relaxation occurs is apparently in the range 0 to 1–2 Myr.

There is evidence that the oceanic lithosphere may continue to relax over longer times. For example, Fig. 3 shows a plot of T_e against age of the lithosphere for seamounts and oceanic islands. The estimates are colour-coded according to age, with the oldest features blue and the youngest red. The plot suggests that older seamounts and oceanic islands have a lower T_e than young ones for a given age of the oceanic lithosphere. Some features (e.g. the 51 Ma Ojin seamount) have a low T_e because they were formed on young lithosphere at the time of loading. Others, however, (e.g. the 95 Ma Atlantis seamount) loaded lithosphere that was already quite old at the time of loading. If the general trend seen in Fig. 3 is representative, it suggests that the lithosphere may relax on timescales as long as 1–2 to 100 Myr.

These inferences of a load-induced stress relaxation in the oceanic lithosphere are suggestive of a viscoelastic behaviour. One possible explanation for the oceanic T_e estimates, therefore, is the thin viscoelastic plate model as described by Nadai (1963). In such a model, the initial flexure is elastic, but viscous effects become increasingly important with time (Fig. 4).

Fig. 5 shows a plot of D against load age for seamounts and oceanic islands that were emplaced on oceanic lithosphere >80 Ma. The observed estimates (filled circles) are from the Atlantic, Indian and Pacific oceans. The calculated curves (solid lines) are based on a thin viscoelastic plate model with an initial elastic thickness, T_0, of 90 km. We chose this value because it is mid-way between the range of estimates of the seismic thickness (70–110 km) of >80 Ma oceanic lithosphere based on surface-wave studies (Nishimura & Forsyth 1989). The figure shows that a thin viscoelastic plate model explains the general decrease that is observed in D with increase in load age. However, no single relaxation time can explain *all* the data. Furthermore, no relaxation time can explain the data in the long term. In particular, the observed decrease in D (as illustrated by the open arrows) appears to be gentler than predicted, suggesting that, rather than the flexed plate approaching the

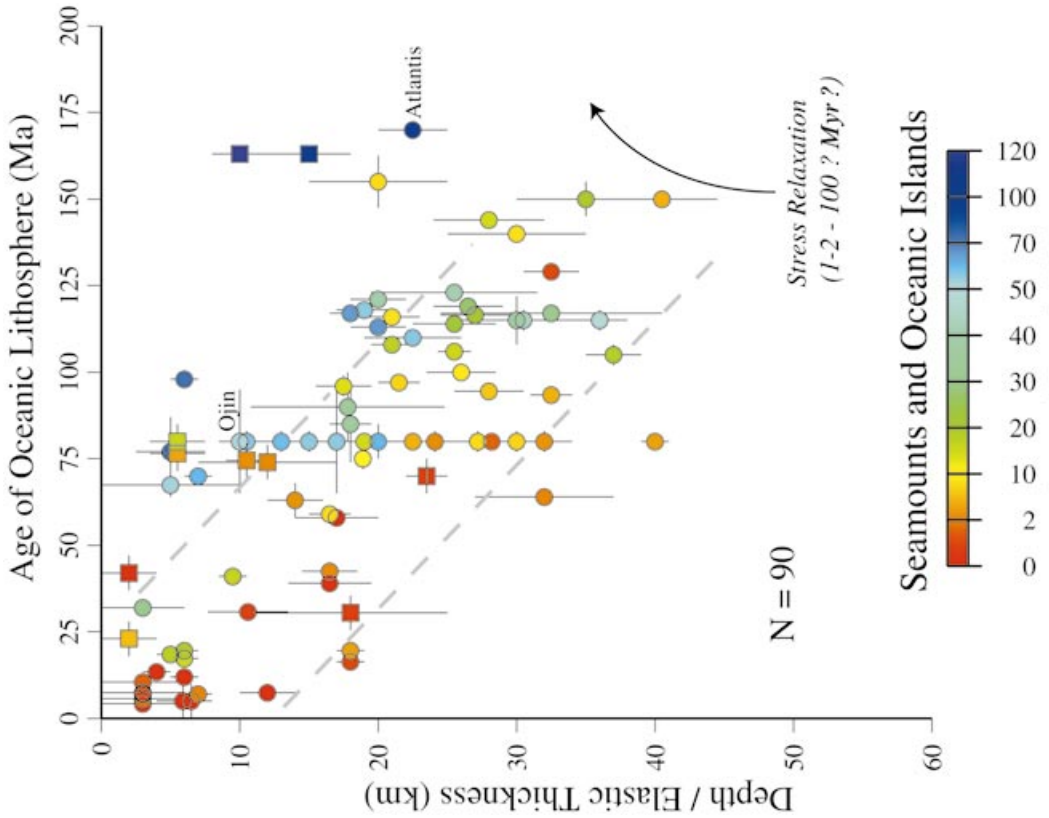

Figure 3. Plot of elastic thickness of the oceanic lithosphere, T_e, against age of the lithosphere at seamounts and oceanic islands. Squares show seamounts and oceanic islands in French Polynesia. Ojin and Atlantis seamounts are discussed in the text. Circles show seamounts and oceanic islands excluding those in French Polynesia. The squares and circles have been colour-coded for age of the load, with reds indicating young ages and blues old ages. The long curved arrow and dashed grey lines schematically illustrate the effect on T_e of a long-term (0–2 Myr) stress relaxation in the lithosphere.

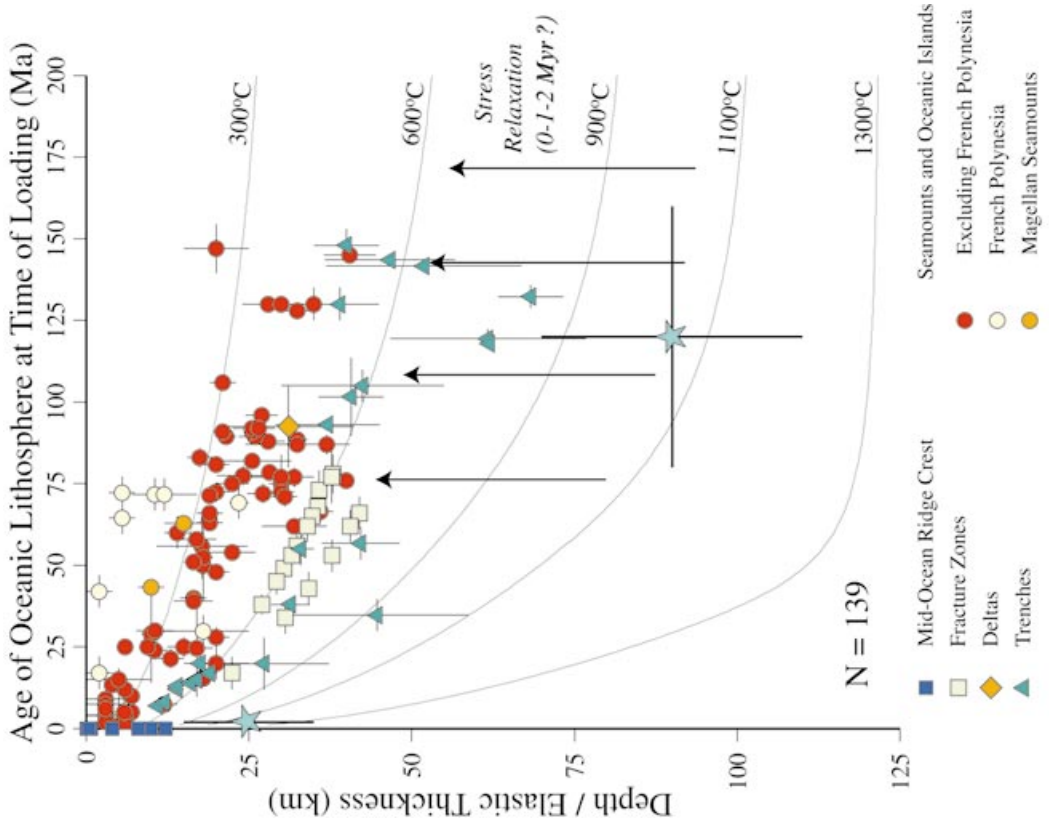

Figure 2. Plot of elastic thickness of the oceanic lithosphere, T_e, against the age of the lithosphere at the time of loading. The isotherms are based on the cooling-plate model of Parsons & Sclater (1977). The seismic thickness is based on Nishimura & Forsyth (1989). Long straight arrows schematically illustrate the effect on T_e of a short-term (0–2 Myr) stress relaxation in the lithosphere.

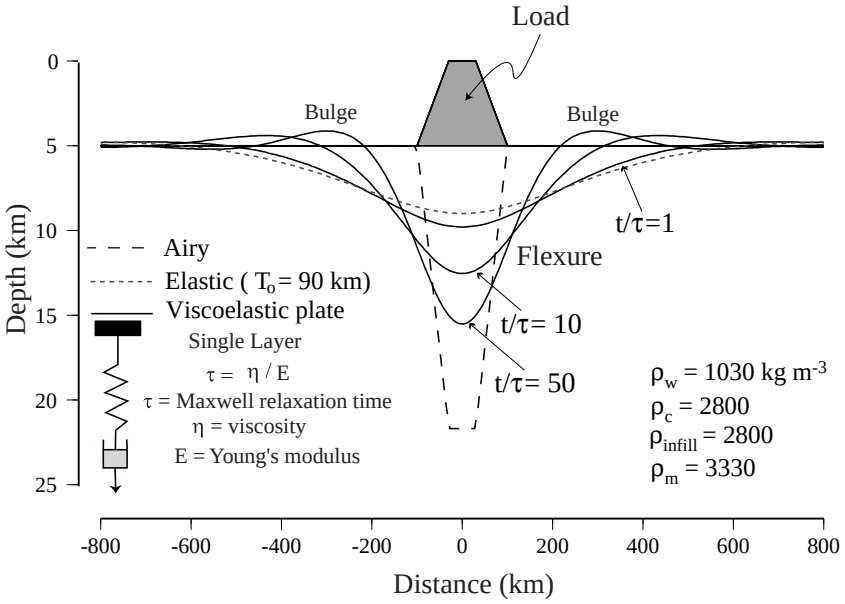

Figure 4. Flexure of a thin viscoelastic plate that overlies an inviscid fluid substratum. The flexure has been computed for an assumed initial elastic thickness, T_0, of 90 km, a Young's modulus of 100 GPa, the load distribution shown, densities of the load, material displaced by the load, infill density and mantle of 2800, 1030, 2800 and 3330 kg m^{-3}, respectively, and a ratio of $t/\tau = 1$, 10 and 50, where τ is the Maxwell relaxation time and t is the age of the load.

limit of great weakness, it approaches a finite strength. However, even when a viscoelastic plate model is used, which includes an initial as well as final elastic thickness (Karner 1982), the observations still cannot be explained.

3 VOLCANIC LOADING OF A MULTILAYERED VISCOELASTIC LITHOSPHERE

The thin elastic and viscoelastic plate models are only approximations to the long-term mechanical behaviour of the lithosphere. They do not incorporate any of the laws for the brittle and ductile deformation of rocks, as determined by the results of experimental rock mechanics. Neither do they explicitly take into account the thermal structure of the lithosphere. A better model, therefore, would be one that incorporates the results of experimental rock mechanics, which show that rocks behave by brittle deformation in the upper crust and that creep in the suboceanic mantle is a thermally activated process.

Bodine *et al.* (1981) constructed a model that incorporated the data from experimental rock mechanics and the thermal structure, and solved for the flexure due to an arbitrarily shaped load. They computed the moment associated with the yield strength envelope, which Goetze (1978) constructed from Byerlee's law for brittle deformation and the Dorn and power law for ductile deformation, and found the equivalent flexure of a purely elastic plate. We follow here, however, the approach of Courtney & Beaumont (1983), and ignore the brittle deformation field. Our reasons for doing this are two-fold. First, the brittle deformation field is still poorly understood. Second, there is little evidence in the flexural moats that flank seamounts and oceanic islands for yielding in the form of normal faulting. Since temperature varies non-linearly with depth in a cooling lithosphere, and viscosity is a strong function of temperature, the problem therefore reduces to being able to calculate the flexure of a *multilayered* viscoelastic plate model which is subject to arbitrarily shaped loads.

3.1 Physical model and governing equations

The response of a multilayered viscoelastic plate to loads can be described (e.g. Zhong 1997) by the following governing equations:

$$\sigma_{ij,j} + \rho g \delta_{i2} = 0\,, \tag{2}$$

$$u_{\bar{i},i} = 0\,, \tag{3}$$

where ρ is the density, g is the gravitational acceleration, $u_{\bar{i}}$ is the velocity (or displacement depending how we define the rheological equation), and σ_{ij} is the stress tensor. Eqs (2) and (3) are the equations of motion and continuity, respectively.

The rheological equation for an incompressible viscoelastic medium (e.g. a Maxwell body) can be written

$$\sigma_{ij} + \frac{\eta}{\mu}\,\dot{\sigma}_{ij} = P\delta_{ij} + 2\eta\dot{\varepsilon}_{ij}\,, \tag{4}$$

where μ and η are the shear modulus and viscosity, respectively, P is the dynamic pressure, ε is the strain tensor and the dot indicates the derivative of a variable with respect to time.

We assume in solving eqs (2)–(4) that both the top and bottom surfaces of the deformed plate are free surfaces. For a given applied load and set of mechanical properties (e.g. viscosity, shear modulus), we can solve the equations either analytically or numerically and calculate how the deformation near the load varies with time. In this paper, an analytical rather than a numerical approach has been followed. This is because we use a linear rheology and are concerned with displacements that are small compared with the plate thickness. A similar approach was followed by Zhong (1997) in his study of the evolution of the long-wavelength topography of orogenic belts.

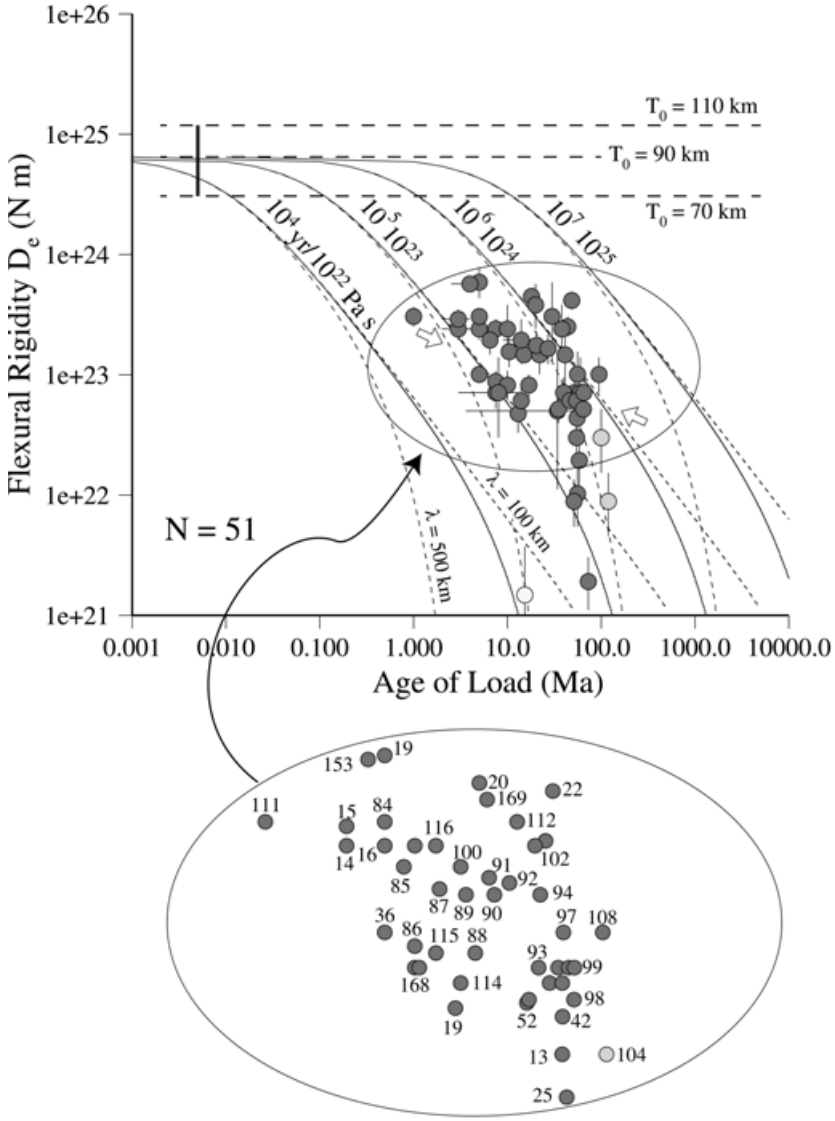

Figure 5. Comparison of observed and predicted flexural rigidity, D, at seamounts and oceanic islands that formed on >80 Ma oceanic lithosphere. Circles show observed values. Dark circles show all values except those for French Polynesia. Light circles show those for French Polynesia. The observations are identified in the expanded plot, based on Table 1. Solid and finely dashed curves show the predicted relationship between D and age of the load based on a thin viscoelastic plate model. The model assumes an initial elastic thickness, T_0, of 90 km and Maxwell relaxation times of 10^4, 10^5, 10^6 and 10^7 yr. Solid curves are for a load with wavelength, λ, of 250 km. Finely dashed curves are for loads with wavelengths of 100 and 500 km. The coarse dashed lines show the initial flexural rigidity based on a T_0 of 70, 90 and 110, the likely range of the seismic thickness of >80 Ma oceanic lithosphere. The unfilled arrows show possible trends in the data.

3.2 Rheology model

Laboratory studies show that creep for most minerals that make up the oceanic lithosphere is a thermally activated process. For example, the general creep law for polycrystalline olivine is given (e.g. Karato & Wu 1993) by

$$\dot{\varepsilon} = A(\sigma/\mu)^n (b/d)^m \exp[-(E+PV)/RT], \quad (5)$$

where A is a pre-exponential factor, σ is the shear stress, b is the length of the Burgers vector, d is the grain size, n is the stress exponent, m is the grain-size exponent, E is the creep activation energy, P is ambient pressure, V is the activation volume, R is the universal gas constant, and T is the temperature. The strain rate, $\dot{\varepsilon}$, is determined by the viscosity, η, and shear stress, σ, and so it follows from eq. (5) that

$$\eta = \frac{\sigma}{2\dot{\varepsilon}} = \eta_{\text{ref}} \exp[(E+PV)/RT], \quad (6)$$

where

$$\eta_{\text{ref}} = \frac{\mu}{2A} (\sigma/\mu)^{1-n} (b/d)^{-m}.$$

As Karato & Wu (1993) and colleagues have pointed out, the rheological parameters for olivine vary widely for different deformation mechanisms and volatile content. For example, in diffusion creep the stress exponent is 1, but it maybe as high as 3–5 for dislocation creep. Similarly, the activation energy varies from 300 to 540 kJ mol^{-1} for 'dry' samples to 240–430 kJ mol^{-1} for 'wet' samples.

Because of uncertainties in the actual deformation mechanism that characterizes the lithosphere, we follow here the approach taken by Courtney & Beaumont (1983) and assume a linear rheology (i.e. the stress exponent is 1). A linear rheology is consistent with the results of Karato & Wu (1993), who point out that dislocation creep may only be important at relatively high temperatures (e.g. at the mid-oceanic ridge), while diffusion creep is important at low temperatures. Since the load ages for seamounts and oceanic islands are relatively large (>1 Ma), the regions in the lithosphere that are undergoing stress relaxation involve a significant portion of its shallow part where the temperatures are relatively low (possibly 600–700 °C). Therefore, diffusion creep is probably a reasonable assumption for the load cases considered here.

If we assume a linear rheology (e.g. eq. 6), the viscosity can be expressed in terms of the reference viscosity η_{ref}, E, P, V, R and T. The parameters P, V, R and T can all be prescribed for the oceanic lithosphere (e.g. Table 2). P is a pressure term which is given by ρgz, where ρ is the average density of the lithosphere, g is the gravitational acceleration, and z is depth; V is the activation volume; and R is the Universal Gas Constant. T is the temperature in degrees kelvin. We assume here that T is given by a cooling plate model (Parsons & Sclater 1977), since this model provides a good description of the variation in depth of the seafloor and heat flow away from a mid-oceanic ridge crest. As Fig. 6 illustrates, the viscosity structure of the oceanic lithosphere that results is very sensitive to temperature, decreasing by >15 orders of magnitude with depth. The maximum rate of decrease is greatest in the uppermost 25–50 km of the lithosphere, with young seafloor showing the most rapid changes at shallow depths, and old seafloor the least rapid.

Table 2. Physical parameters used in the multilayered viscoelastic model calculations.

Parameter	Value
Crust and mantle shear modulus	50 GPa
Thickness of the mantle	2900 km
Poisson's ratio	0.5
Density of the crust	2800 kg m^{-3}
Density of the mantle	3330 kg m^{-3}
Creep activation volume	5×10^{-6} m^{-3} mol^{-1}
Gravitational acceleration	9.81 m s^{-2}
Universal Gas Constant	8.3 J mol^{-1} $°K^{-1}$

Once P, V, R and T are prescribed, the only unknown parameters are η_{ref} and E. We therefore used eq. (6) to construct viscosity profiles for the lithosphere based on various values of η_{ref} and E. In each calculation, the viscosity profile with depth was approximated to a number of layers (in most cases, 16–17) of constant viscosity. The layers were divided such that the viscosity ratios between two adjacent layers were always smaller than 5. Furthermore, the maximum viscosity was limited to 10^{28} Pa s, since higher viscosities had no influence on the calculations. We then calculated the response of the multilayered viscoelastic model to loads of various shape, dimensionality (i.e. 2-D or 3-D), duration and thermal age of the lithosphere at the time of loading.

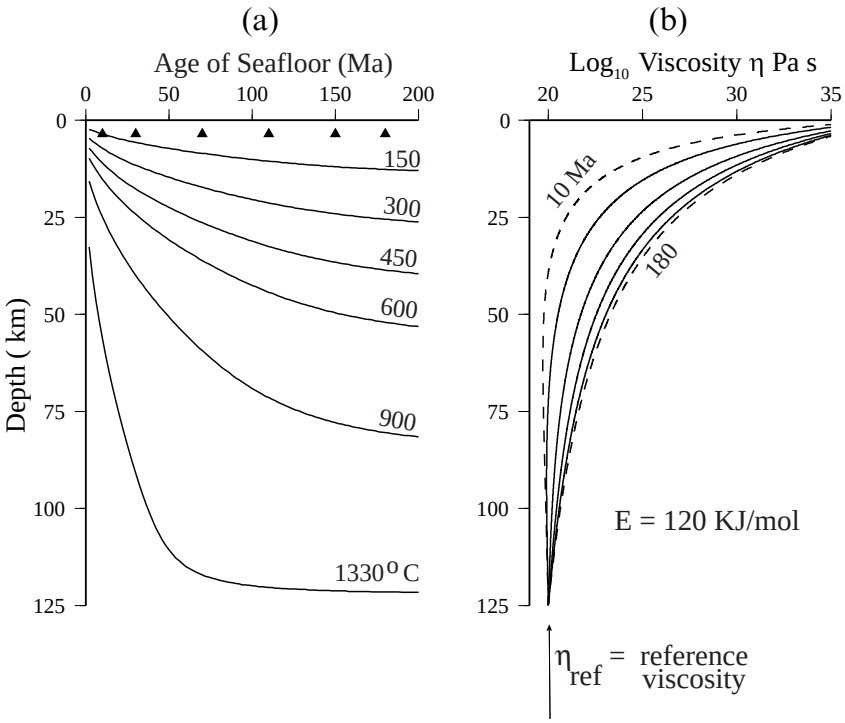

Figure 6. Plot of temperature structure and viscosity of the oceanic lithosphere as a function of age. (a) Depth versus temperature based on a plate-cooling model (Parsons & Sclater 1977). Filled triangles indicate ages at which the viscosity structure has been computed in (b). (b) Depth versus log of the viscosity based on a model in which creep in the mantle is a thermally activated process. The calculations assume an activation energy, E, of 120 KJ mol^{-1} and a reference viscosity, η_{ref}, such that the viscosity in the upper mantle (at a depth of 125 km) is 10^{20} Pa s.

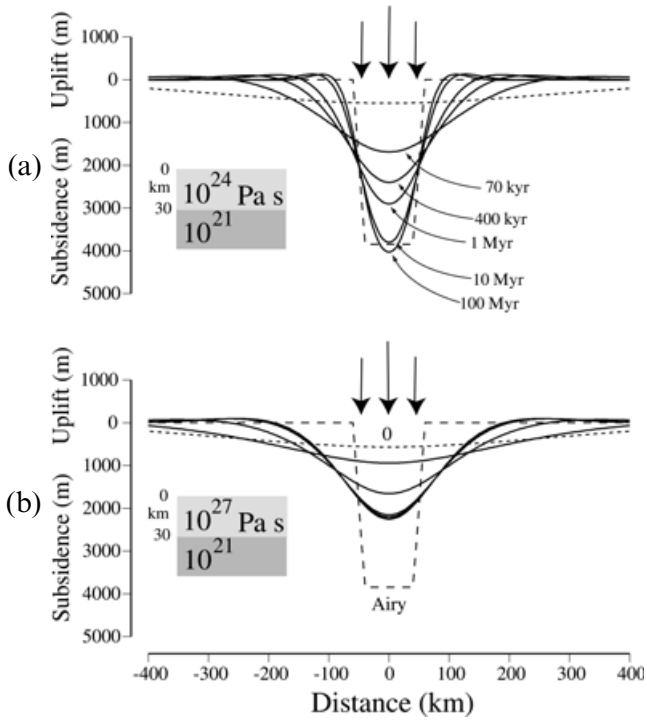

Figure 7. Flexure of a two-layer viscoelastic plate model. Solid lines show the predicted flexure at 70 kyr, 400 kyr, 1 Myr, 10 Myr and 100 Myr following load emplacement. Narrow dashed lines show the initial (elastic) flexure. Wide dashed lines show the response of an Airy-type model. The calculated curves assume a 30 km thick upper layer and a lower layer with a viscosity of 10^{21} Pa. (a) Low-viscosity upper layer. (b) High-viscosity upper layer.

3.3 Comparisons of the multilayered viscoelastic model with the thin elastic and viscoelastic plate models

Before comparing the calculated response with predictions, it is necessary to first validate the multilayered viscoelastic model. One way to do this is by comparison with the predictions of the thin elastic and viscoelastic plate models. Because these models are, in effect, two-layer models with either an elastic or viscoelastic upper layer that overlies an inviscid lower 'layer', we can compare their response with the special case of a two-layer multilayered viscoelastic model.

Fig. 7 shows the flexure of a two-layer viscoelastic plate that is loaded on its surface by a 'standard'-sized[1] seamount. Two cases are illustrated: one with a high-viscosity upper layer (Fig. 7b) and the other with a low-viscosity layer (Fig. 7a). An upper-layer thickness of 30 km and a lower-layer viscosity of 10^{21} Pa s are assumed to apply in both cases. Since the viscosity of the lower layer is *less* than that of the upper layer in both cases, the plate relaxes on loading *from the base upwards*. The flexure immediately beneath the load increases with time, reaching its maximum value after the longest time has elapsed. In the case of the low-viscosity upper layer, the flexure increases rapidly and approaches the predictions of the Airy model after 10 Myr. In contrast, the case of the high-viscosity upper layer does not approach the Airy case, even after 100 Myr.

[1] Defined by a basal radius of 40 km, a top radius of 20 km and a height above the surrounding seafloor of 4 km.
[2] Data source: http://www.expet.gps.caltech.edu/Hawaii_project.html.

The maximum flexure of the two-layer multilayered viscoelastic models is compared with the predictions of the elastic and viscoelastic plate models for a range of load ages in Fig. 8. The flexures of the thin elastic and viscoelastic plate models were computed with $T_e = 30$ km and a viscosity of 10^{24} Pa s, respectively. In the thin elastic model, the flexure does not vary with time. The flexure of the viscoelastic model is the same as that of the elastic model for times < 0.1 Myr. For longer times, however, it deviates, approaching the predictions of an Airy model after 10 Myr.

Fig. 8 shows that the predictions of the model with a high-viscosity upper layer agree well with the predictions of an elastic plate model, at least for long load ages. The main difference is at short load ages. This is because in the two-layer multilayered viscoelastic model the high-viscosity upper layer is underlain by a lower-viscosity layer. The model therefore relaxes on short, as well as long, times. In contrast, the elastic model assumes that the plate is underlain by an inviscid fluid. Hence, there is no time-dependence in the flexure of an elastic model.

The model with a low-viscosity upper layer agrees well with the predictions of the viscoelastic plate model. Again, the agreement is closest for long ages (i.e. > 0.1 Myr) of loads. However, the agreement depends on the viscosity that is assumed for the underlying layer. A viscosity of $< 10^{21}$ Pa s is well explained, whereas a viscosity of $> 10^{22}$ Pa s is poorly explained. The reason for this is that, in the two-layer viscoelastic model, the lower layer, like those in the elastic and viscoelastic plate models, is relatively weak. Apparently, if the viscosity of the lower layer is low enough (i.e. $< 10^{21}$ Pa s), the plate behaves

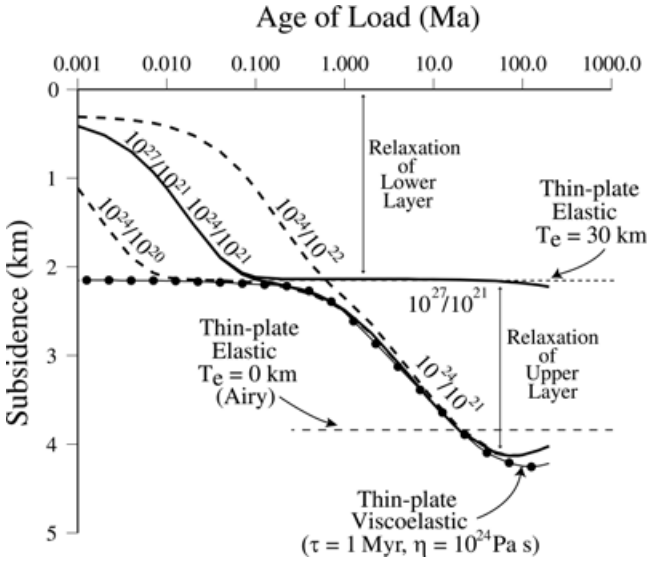

Figure 8. Comparison of the calculated flexure for a thin plate elastic and viscoelastic plate model with that of a two-layer viscoelastic plate model. The calculations show the maximum subsidence beneath the centre of a seamount-type volcanic load as a function of load age. Heavy solid and dashed lines show the predictions of the two-layer viscoelastic model. The first number in the label refers to the viscosity of the upper layer, and the second to the lower layer. Light short-dashed lines show the prediction of a thin elastic plate model with $T_e = 30$ km. Light long-dashed lines show the Airy response (i.e. $T_e = 0$ km). Filled circles and the light solid line show the prediction of a thin plate viscoelastic model with a Maxwell relaxation time of 1 Myr (equivalent to a viscosity of 10^{24} Pa s).

in a similar way to a thin elastic or viscoelastic plate that is underlain by an inviscid fluid.

These comparisons demonstrate that the widely used thin elastic and viscoelastic plate models can be considered as special 'end-member' cases of a multilayered viscoelastic model. A two-layer viscoelastic model with an upper layer that has a high viscosity (i.e. 6 orders of magnitude greater than that of the lower layer) is essentially behaving as an elastic plate overlying an inviscid fluid for timescales in the range 0.1–100 Myr (Fig. 8). At longer times, the subsidence will differ from that in the elastic plate model, unless a higher viscosity is assumed for the upper layer. Moreover, a two-layer model with a low-viscosity upper layer is essentially behaving as a viscoelastic plate over the same timescales, provided that the viscosity of the lower layer is low enough (i.e. at least 3 orders of magnitude lower than that of the upper layer).

3.4 Sensitivity to load size

As a number of workers have pointed out (e.g. Lambeck & Nakiboglu 1981), the response of a viscoelastic plate that overlies an inviscid fluid depends on load size, with greater flexures being predicted for wider loads than for small ones. Hence, there should be a dependence of T_e on load size. This is illustrated in Fig. 5. The figure suggests that, while the flexural rigidity and, hence, T_e of a plate that supports a load with a wavelength of 1000 km differs little from that of a plate that supports a load with a wavelength of 100 km for small load ages, departures occur as the load age increases. The departures become most significant when the load age exceeds that of the relaxation time.

In contrast, the multilayered viscoelastic model shows only a weak dependence of T_e on load size. This is because the amount of stress relaxation in this model becomes insignificant the longer that a load remains on the plate. After a few million years, for example, the stress concentrates in the shallow uppermost part of the lithosphere, where the viscosity is high. The plate therefore behaves more elastically on long timescales such that the flexure beneath a load, irrespective of its size, will not change significantly with time. However, T_e will depend on size when the load is young and the amount of stress relaxation is significant.

A lack of dependence of T_e on load size is also seen in the observations. We estimated, for example, the size of some 81 seamounts and oceanic islands where T_e has been determined, using both surface ship bathymetry and GEBCO bathymetric charts as a data source. In each case, the size of a feature is expressed as a top radius, a base radius, and a peak height. The radii are based on the degree of circularity of the volcanic edifice. In those cases where the edifice forms more of a submarine ridge, the radii are minimum estimates. The peak height is the mean height of the volcanic feature (i.e. the submarine edifice and, where applicable, the subaerial part of the volcano) above the surrounding 'normal' depth of the seafloor. Plots of the base radius against peak height are shown in Fig. 9. Although there is a tendency for smaller seamounts and oceanic islands to be associated with younger seafloor than large ones, Fig. 9(a) shows a generally weak dependence between size and seafloor age. There is a similar weak dependence of size on load age (Fig. 9b). Finally, Fig. 9(c) shows an apparent lack of dependence of size on T_e.

If a trend exists at all in Fig. 9, it suggests that T_e is higher for large seamounts and oceanic islands than for small ones. This cannot be attributed to the effects of stress relaxation. Rather, it is probably caused by the fact that many of the largest seamounts and oceanic islands are found on old seafloor, and old seafloor tends to have a higher T_e than young seafloor.

4 ESTIMATES OF ACTIVATION ENERGY AND REFERENCE VISCOSITY

We have used the multilayered viscoelastic model to compute the flexure that would be expected for loads that are emplaced on the surface of oceanic lithosphere of different ages. Although the flexure could be compared directly with observations, there are only a few localities (e.g. Hawaii, Canary Islands, Réunion) where seismic techniques have directly imaged the flexure of the oceanic crust in the vicinity of large volcanic loads. In most localities, the flexure is inferred from gravity and geoid observations. We therefore express the modelled flexure in terms of T_e or the equivalent flexural rigidity, D, and then compare these values, rather than the actual flexural deformation, with observations.

A difficulty in thin viscoelastic plate models lies in specifying the initial elastic response. In our multilayered model, the initial elastic response is determined by the shear modulus, the load size (i.e. amplitude and wavelength), and the thickness of the mantle. It is therefore independent of the viscosity structure. Since the mantle is relatively thick, the T_e obtained from the initial (i.e. $t=0$) elastic response is large also. The T_e then gets progressively smaller with time as the stress that accumulates in the mantle relaxes and the thickness of the lithosphere that supports a load decreases from its short-term seismic thickness to its long-term thickness. We caution, however, that the calculated T_e after a few to a few hundred seconds may not actually correspond to the seismic thickness. This is because we have over-simplified the elastic properties of the mantle. These simplifications should not, however, affect the long-term behaviour of the lithosphere.

Fig. 10 compares observed and predicted estimates of the flexural rigidity at seamounts and oceanic islands. The observations are based on the same data set as used in Fig. 5 and represent seamounts and oceanic islands that are now located on >80 Ma oceanic lithosphere. We chose such an old age range for two reasons. First, the seismic thickness and, hence, the initial elastic thickness of old oceanic lithosphere is unlikely to vary significantly. Second, the increase in the thickness of the plate as it cools and, hence, its effect on the load-induced stress relaxation, will also be small. The observations have been colour-coded according to the age of the lithosphere at the time of loading, with seamounts and oceanic islands that formed on young lithosphere red and those that formed on old lithosphere blue. The calculated flexural rigidity (solid lines) is based on the predictions of a multilayered viscoelastic model with $E=120$ KJ mol^{-1} and $\eta_{ref}=10^{20}$ Pa s, and ages for the lithosphere at the time of loading of 30, 70, 110 and 150 Ma. This range encompasses the observations (see inset in Fig. 10) that show a distinct peak in the age of the oceanic lithosphere at the time of loading of 70–90 Ma. Fig. 10 shows that the predicted flexural rigidity for an age of the lithosphere at the time of loading of 70 Ma explains the general trend and passes approximately through the mid-point of the observed data. If we take

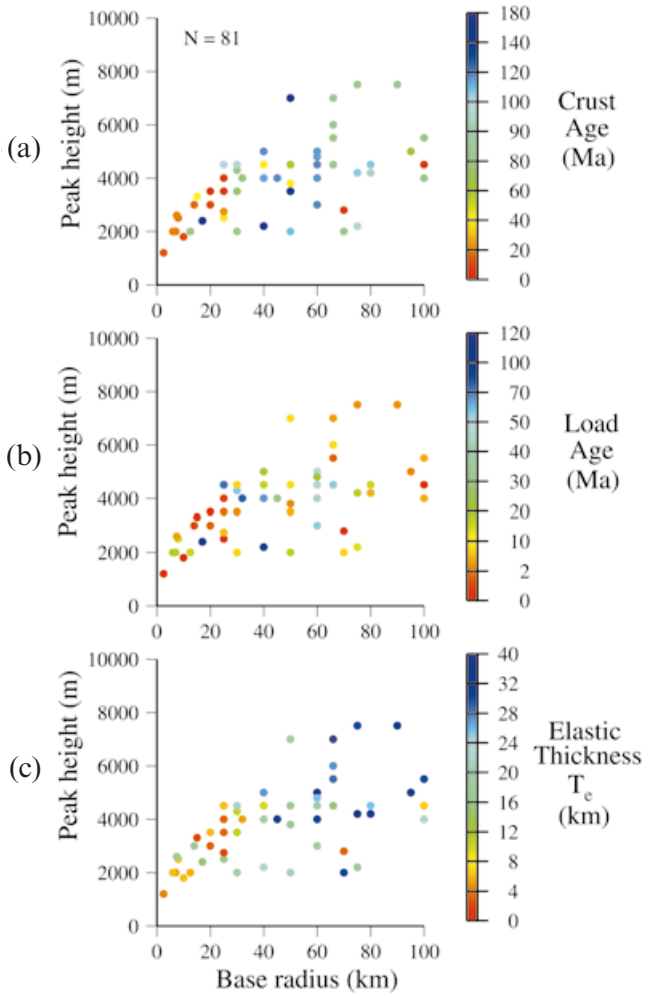

Figure 9. Plot of the peak height against basal radius for the 81 seamounts and oceanic islands where estimates of crust age, load age and T_e are available. The height and basal radius estimates are based on GEBCO maps and shipboard bathymetry profiles. The estimates have been colour-coded according to (a) age of the oceanic crust, (b) load age, and (c) T_e.

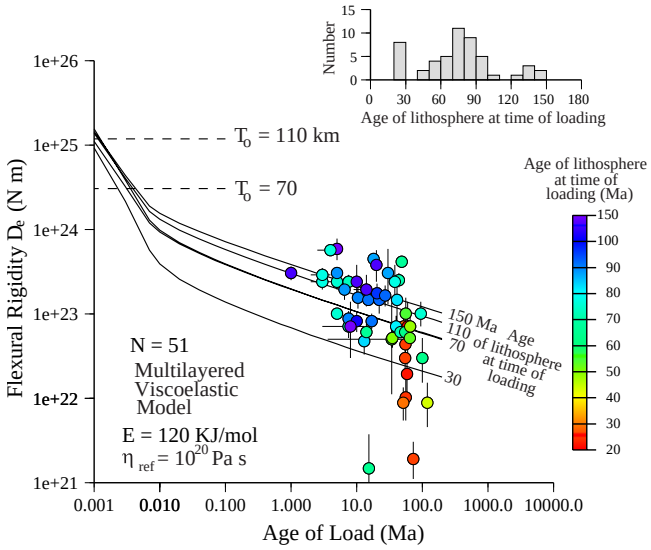

Figure 10. Comparison of observed and predicted flexural rigidity, D, at seamounts and oceanic islands that formed on >80 Ma oceanic lithosphere. Circles show observed values which have been colour-coded according to the age of the lithosphere at the time of loading. Solid curves show the predicted relationship between D and age of the load based on a multilayered viscoelastic plate model. The model assumes an activation energy, E, of 120 kJ mol^{-1}, a reference viscosity of 10^{20} Pa s, and ages of the oceanic lithosphere *at the time of loading* of 30, 70 (heavy solid line), 110 and 150 Ma. The inset histogram shows a peak in the ages of the lithosphere at the time of loading in the observed data at 70–90 Ma.

into account the range of ages of the lithosphere at the time of loading, then some 90 per cent of the observed estimates of flexural rigidity fall within the window of the calculated values. Moreover, there is a hint of an alignment of observations that have a similar age of the lithosphere at the time of loading along the predicted curves.

While a parameter pair of $E = 120$ KJ mol^{-1} and $\eta_{ref} = 10^{20}$ Pa s therefore generally explains the observed flexural rigidity (and hence, T_e) estimates, there are trade-offs. Fig. 11 shows, for example, that the flexural rigidity estimates in Fig. 10 could be equally well explained by either a higher reference viscosity and lower activation energy or a lower viscosity and a higher activation energy.

There are indications that E and η_{ref} may vary regionally. For example, some 10 per cent of estimates of flexural rigidity fall outside the range of the predicted curves. Most notable are two estimates from the Hawaiian Ridge (Midway, Oahu), two from the Emperor seamounts (Koku), and two from Bermuda which are associated with a higher flexural rigidity than expected, and one estimate from French Polynesia (Maria) and one from the Atlantic (Corner) which are associated with lower values. These anomalous values may indicate regional variations in either the creep activation energy or the basal viscosity of the lithosphere or both of these parameters Alternatively, they may represent regional variations in the temperature structure of the lithosphere.

The reference viscosity of $\eta_{ref} = 10^{20}$ Pa s that is assumed in Fig. 10 can be considered as a basal viscosity to the lithosphere or, equivalently, an estimate of the viscosity of the uppermost mantle. Postglacial rebound studies (e.g. Wu & Peltier 1983; Vermeersen *et al.* 1998) suggest that 10^{20} Pa s is a reasonable estimate of the viscosity of the uppermost mantle beneath tectonically quiet continental regions. If this viscosity is also appropriate for the suboceanic mantle, as the work of Mitrovica & Forte (1997) suggests, then the comparison of observed and predicted flexural rigidities illustrated in Fig. 10 suggests a 'best-fit' creep activation energy for the mantle of 120 KJ mol^{-1}. This is less than the 200–250 KJ mol^{-1} deduced by Courtney & Beaumont (1983) using the same viscosity, but an older T_e data set. It is also smaller than has been deduced from laboratory studies of polycrystalline samples of olivine, the major mineral constituent of the mantle. Karato & Wu (1993), for example, have pointed out that the activation energy for 'wet' and 'dry' samples ranges from 240 to 300 KJ mol^{-1} for linear diffusion creep to 430–540 KJ mol^{-1} for non-linear dislocation creep. Hence, the discrepancy between the laboratory and 'field-based' results is up to a factor of 2–4.

At present, we do not know the cause of the discrepancies between these field-based and laboratory estimates. If, as Karato & Wu (1993) suggest, diffusion creep is a more likely

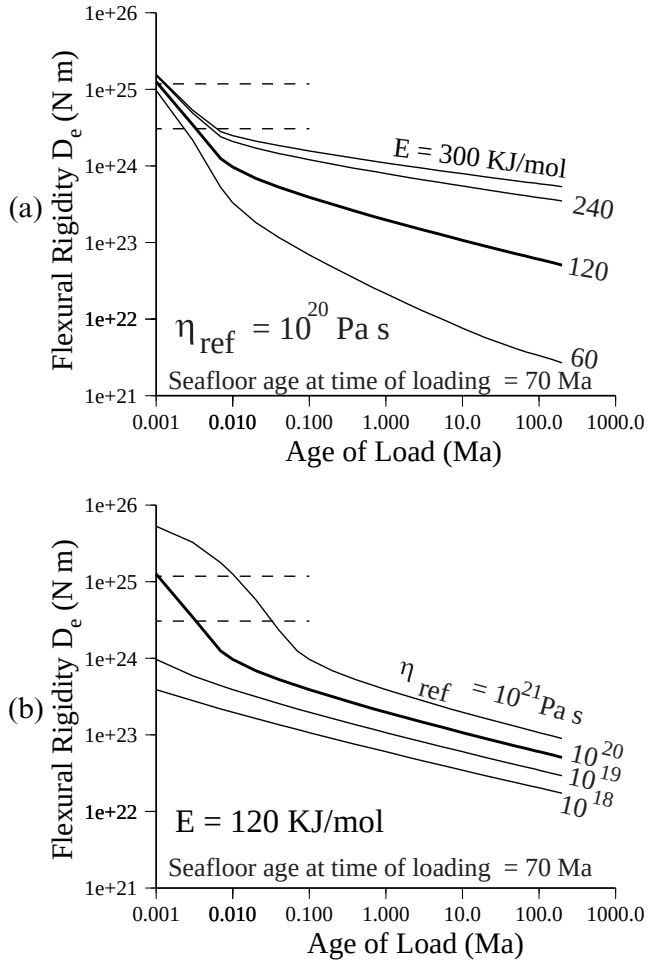

Figure 11. Sensitivity of the relationship between flexural rigidity, D, and load age for a multilayered viscoelastic model to (a) activation energy and (b) reference viscosity. The horizontal dashed lines correspond to an elastic thickness of 70 km (lower line) and 110 km (upper line).

deformation mechanism beneath 20–150 Ma old oceanic lithosphere than dislocation creep, which is probably limited to the high-geothermal-gradient regime of the mid-oceanic ridge, then the discrepancy reduces to a factor of 2. The rest of the discrepancy may be caused by uncertainties in the role of volatiles, with our results indicating a greater role of water fugacity (or water content) in the suboceanic mantle than was previously thought. Water may significantly decrease mantle viscosity, which would lead to a higher activation energy. Hirth & Kohlstedt (1996), for example, have suggested that there is enough water beneath a mid-oceanic ridge to lower the viscosity of the suboceanic mantle from 10^{20} to 10^{18} Pa s. The problem is that the flexural rigidity is, as Fig. 11 clearly shows, more sensitive to the activation energy than to the mantle viscosity, and so we cannot determine how much lower the mantle viscosity would need to be in order to explain the T_e observations.

The most obvious difference between the field and laboratory estimates is the much lower strain rates that are involved in flexural loading, and so we believe, in the absence of any other information, that this factor is the most probable source of the discrepancy.

5 IMPLICATIONS

We have shown that a multilayered viscoelastic model predicts that the flexure immediately beneath a seamount-type volcanic load will increase with load age. Initially (i.e. $t = 0$ Myr) the flexure is elastic (e.g. Fig. 12). As the load ages, stresses in the underlying lithosphere relax rapidly, such that ~ 50 per cent of the subsequent flexure is reached within 10 ka. Subsequent changes in flexure are slow as stresses tend to concentrate in the high-viscosity uppermost layer of the lithosphere. The net result is that it takes a further 100 Myr to reach the same amount of flexure as occurred during the first 10 kyr of loading.

These changes in flexure with load age have geological implications. On long timescales there is little change in the amplitude and wavelength of flexure. Hence, there is a certain 'permanence' to the observations of flexure (e.g. gravity and geoid anomalies, seafloor topography and the flexed surfaces of the top and base of the crust) such that they may be used with confidence (e.g. Watts *et al.* 1980) to estimate the tectonic setting of a bathymetric feature, and in some cases, its age. On short timescales, however, the models suggest that the flexure will change quite rapidly. We examine here some of the implications of these changes for the subsidence and uplift history of active and drowned oceanic islands as well as the stratigraphy of the flexural moats that flank them.

5.1 Subsidence and uplift history of the Hawaiian Islands

The Hawaiian Islands comprise a chain of volcanoes which systematically increase in age from the youngest, Kilauea, on Hawaii Island (Clague & Jarrard 1973). The island comprises a succession of subaerially erupted alkalic basalts which range in age from 0 to 0.5 Ma. Successive volcanoes have built up on the flanks of older volcanoes, such that the youngest, Kilauea, occupies the greatest surface area of the island while the oldest, Mahukona, occupies the smallest. While subaerial basalts make up the entire surface outcrop, their volume is small (< 5 per cent) when compared with that of the underlying submarine edifice.

Although the submarine edifice has not yet been drilled, extrusion rates suggest that the main shield-building phase of a Hawaiian volcano is rapid and may be completed within 0.5–1.5 Ma. Despite this rapid build-up, and probably as a consequence of it, there is evidence that Hawaii has been subsiding by significant amounts. Tide-gauge data (Moore 1970), for example, indicate that Hawaii has been subsiding relative to Oahu at rates of up to 4.8 mm yr^{-1} during the past 90 years. Maui, which is located mid-way between Hawaii and Oahu, appears to have subsided at rates of 1.7 mm yr^{-1} during the same period. Furthermore, historic and archaeological data (Apple & Macdonald 1966) suggest that Hawaii has been subsiding at rates of about 3 mm yr^{-1} since Captain Cook's last visit to the island in 1750.

There is evidence that Hawaii has been subsiding on even longer timescales (Moore & Fornari 1984; Moore & Campbell 1987; Ludwig *et al.* 1991). Detailed bathymetric data, for example, indicate that northwest of Hawaii there is a series of reef terraces at depths of 100–1300 m which formed at sea level during periods of relative shoreline stability. Samples of a 204–219 m deep reef yield radiocarbon ages of 13.25 ka, while samples of a 580 m deep reef yield ages of 255 ka (Moore

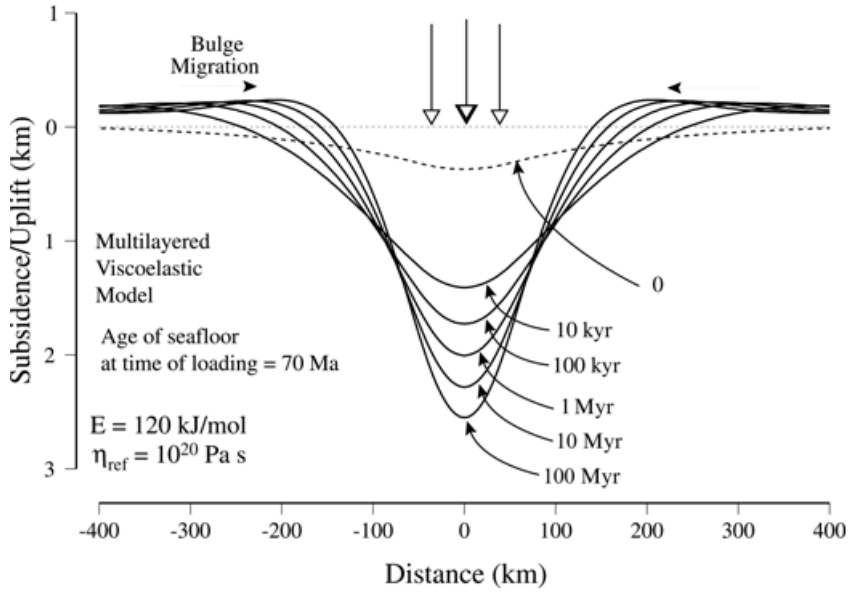

Figure 12. Predicted flexure for a seamount-type volcanic load that forms on 70 Ma oceanic lithosphere. The long-dashed line shows the initial (i.e. $t=0$) flexure. Solid lines show the flexure at 10 kyr, 100 kyr, 1 Myr, 10 Myr and 100 Myr. The predictions are based on the 'best-fit' parameter pair of activation energy and reference viscosity that explain the flexural rigidity estimates in Fig. 10.

& Campbell 1987). Together, these data suggest subsidence rates of 1.8 mm yr^{-1} for the past 13.25–255 ka Ludwig *et al.* (1991), who sampled even deeper terraces, suggest rates as high as 2.8 mm yr^{-1} over the past 0.5 Ma. These rate estimates are in broad agreement with the results of Uranium-based age dating of subaerial basalts in the scientific drill hole in the harbour of Hilo, Hawaii.

That the terrace rates reflect the subsidence of the island of Hawaii *as a whole* is suggested from a comparison of the ages of the reef terraces northwest of Hawaii with terraces of a similar age to the south of Lanai and east of Maui, two older islands that are now several tens of kilometres 'upstream' of Hawaii. These data suggest that individual reef terraces are tilted (Moore & Campbell 1987) towards the southeast and that they dip in towards the centre of the Hawaii Island load.

While the island of Hawaii has been subsiding, older islands 'upstream' have experienced uplift. Grigg & Jones (1997), for example, have used sea-level indicators such as corals, beach deposits, wave-cut notches, and wave-eroded terraces to document the amount of uplift that has occurred on Oahu, Lanai and Molokai during the past 0.5 Myr. Their data suggest systematic differences in the timing of the uplift along the islands. The uplift on Oahu, for example, spans 100–500 ka, suggesting that it was probably in progress quite soon after completion of the main submarine phase of shield building on Hawaii. In contrast, Lanai experienced uplift over the range of 150–250 ka, which is well into the subaerial phase on Hawaii. Since Oahu is furthest from Hawaii at the present day and Lanai is the nearest, the uplift data suggest that during the past 0.5 ka a flexural bulge may have migrated along the crest of the Hawaiian Islands, affecting Oahu first and Lanai most recently.

We have used the multilayered viscoelastic model to investigate whether the general pattern of subsidence and uplift on Hawaii and upstream islands might be caused by some form of load-induced stress relaxation. Unfortunately, the multiple loading history of the islands precludes a detailed comparison of the model and observations. However, some insight into the relative role of stress relaxation can be obtained if we assume that (1) the submarine edifice of Hawaii is the primary load on the oceanic lithosphere, it formed rapidly, and was essentially completed by 0.5 Ma; (2) the weight of the subaerial load that was added subsequent to 0.5 Ma was small in comparison with that of the submarine load; and (3) the lithosphere that underlies Hawaii responds to loads in a manner similar to that in which a multilayered viscoelastic plate would in which the thermal structure is prescribed by 80 Ma oceanic lithosphere and the mechanical structure is determined by a creep activation energy of 120 KJ mol^{-1} and a basal viscosity of 10^{20} Pa s. With these assumptions we may use the multilayered model to predict the subsidence and uplift history of pre-existing islands that followed the main phase of volcanic loading at Hawaii.

Fig. 13 compares the observed subsidence and uplift with the predictions based on a multilayered viscoelastic model. The figure shows that the uplift data on Lanai can be quite well accounted for by the model. If $E=120$ KJ mol^{-1}, then a reference viscosity $<10^{20}$ Pa s predicts too large an uplift, while a viscosity $>10^{20}$ is too small. A reference viscosity of 10^{20} explains the data reasonably well and predicts an 'emergence' age of about 350 ka for the island. Prior to this, Lanai would have been in Hawaii's flexural moat and would have been subsiding. The age of emergence is in good agreement with data from reef terraces which suggest that subsidence at Lanai ceased about 320 ka (Moore & Campbell 1987). The fact that the uplift data on Lanai cluster around 200 ± 25 ka is, however, puzzling. According to our multilayered model, uplift should have been spread out evenly between the time of emergence and the present day. One possible explanation is that the uplift deposits are of tsunami origin. However, as Grigg & Jones (1997) point out, the uplift on neighbouring islands (e.g. Molokai) shows clear evidence of a continuous uplift and hence we favour a tectonic origin for the uplift on Lanai.

More difficult to explain by our model is the subsidence history of Hawaii itself. There does not appear to be a problem, however, with explaining the older, deeper, terrace data. For

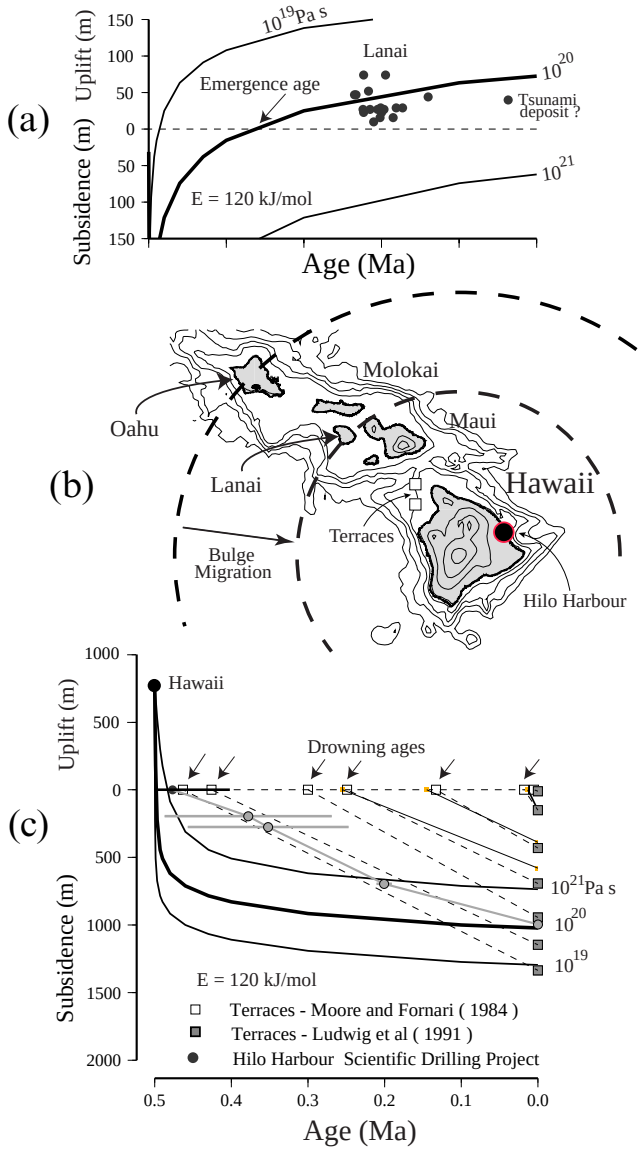

Figure 13. Comparison of the predictions of the multilayered viscoelastic model with observations of uplift and subsidence in the Hawaiian Islands. Thick lines show predictions based on a multilayered viscoelastic model with $E=120$ KJ mol^{-1} and a reference viscosity of $10^{19}-10^{21}$ Pa s. (a) Lanai Island. Solid circles show uplift data based on Grigg & Jones (1997). The data point at 70 ka, -30 m may be a tsunami deposit. (b) Location map showing the Hawaiian Islands. Dashed lines schematically illustrate the crest of Hawaii's flexural bulge as it migrates from Oahu to Lanai. (c) Hawaii Island. Open and filled squares show the depths of dated submarine terraces. Filled circles show the depths of dated subaerial lava samples[2] from the scientific drill hole in Hilo Harbour, Hawaii

example, a model (Fig. 13) in which the 950 m deep terrace was once a 750 m high island which then subsided while above sea level, drowned, and then subsided below sea level can explain the magnitude of the observed total subsidence. The problem is that the subsidence of the younger, shallow, terraces is too rapid to be explained by the model. This is confirmed when examining the data from the scientific borehole in Hilo harbour.

Several factors may contribute to the poor fits to the subsidence data. Like a number of other hot-spot-generated islands, Hawaii is associated with a broad mid-plate swell which has been explained (e.g. Sleep 1992) either as due to thermal rejuvenation of the lithosphere or by dynamic effects of an underlying plume. Irrespective of the cause, the uplift associated with swell formation may compete with the load-induced stress relaxation such that the loading subsidence is generally 'flatter' overall, being less steep early on and steeper later on. Another possibility is that we have over-simplified Hawaii's loading history. We do not know, for example, the detailed growth history of the island during the submarine shield-building phase. Undoubtedly there was subsidence throughout this phase. It is difficult, however, to see how this subsidence could explain our data because it would have been essentially complete by the 0.5–1.5 Myr that we estimate that it took to form the submarine edifice of the island. More likely is some form of load-induced subsidence during the subaerial loading phase. The problem here is that we do not know the loading history for this phase of volcano building either.

5.2 Atolls, guyots, and thermal rejuvenation of the lithosphere

In some respects, Hawaii is an unusual island in that it has undergone large amounts of subsidence yet remains above sea level. This is because the island is relatively young, it sits astride a mid-plate swell, and is associated with a deep-seated high-bouyancy-flux mantle plume. Eventually, of course, Hawaii will drown. We see, for example, that the average elevation of the Hawaiian Islands systematically decreases along the chain from about 3.5 km on Hawaii to <0.5 km on Kauai. Although some of the elevation decrease can be attributed to mass wasting processes such as those associated with large-scale lateral collapse, the systematic nature of the decrease suggests other, tectonic, controlling factors.

Probably the best examples that we have today of drowned volcanic islands are atolls. These features are built up mainly of coral which, typically, form a concentric reef that grows on the rough surface of a volcano flank. Since reefs build to sea level, their thickness provides information on how volcanic islands subside following the cessation of volcanism. Fig. 14 shows that the thickness of fringing reefs at a number of atolls in the Micronesia, Society, Comores, and Gambier (Menard 1983) increases with volcano age. The reef thickness of the five youngest drowned volcanic islands (i.e. ages in the range 0.5–5 Ma), for example, is in the range 250–350 m, as compared with the older islands of Ponope, Mangareva and Truk which have 600–1100 m thick reefs.

Menard (1983) argued that the reef thickness and, hence, subsidence of drowned oceanic islands was caused by thermal cooling of the underlying lithosphere. The subsidence, however, is rapid, and, as Fig. 14 shows, would require that the underlying oceanic lithosphere is thermally re-set to that of a mid-ocean ridge. This implies a zero age for the lithosphere at the time of loading, which is significantly less than the expected age, which ranges from 85 Ma for Moorea in the Society islands to 167 Ma for Truk in Micronesia.

We believe, however, that the rapid subsidence of drowned volcanic islands is more likely to be a result of a load-induced stress relaxation than thermal rejuvenation. Fig. 14 shows that a multilayered viscoelastic model with $E=120$ KJ mol^{-1} and $\eta_{\mathrm{ref}}=10^{20}$ Pa s provides a plausible explanation for the subsidence, especially when it is considered that the volcanic 'core' of each atoll plotted in Fig. 14 could have had a different

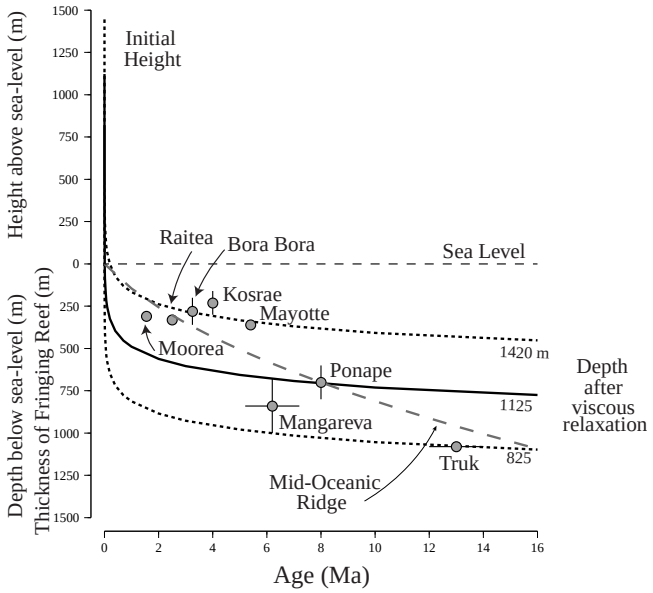

Figure 14. Plot of the thickness of the fringing reefs at atolls as a function of volcano age. Filled circles show observed thickness and age based on the compilation of Menard (1983). The solid line shows the predicted subsidence based on a multilayered viscoelastic model with $E=120$ KJ mol^{-1}, a reference viscosity of 10^{20} Pa s and an original volcano height of 1225 m. The thick short-dashed lines show the predicted curve shifted so as to pass through the data points for Bora Bora and Truk. The thick long-dashed line shows the subsidence that would be expected if a seamount had built up to sea level on oceanic lithosphere of zero age (i.e. a mid-oceanic ridge) and then subsided with age.

starting elevation. The figure shows that, when the age of the lithosphere at the time of loading is taken into account, the thickness of individual fringing reefs can be explained by a multilayered viscoelastic model for starting elevations that are in the range 800–1700 m.

We do not therefore need to invoke thermal rejuvenation of the lithosphere in order to explain the rapid subsidence of atolls. While this does not mean we can discard the hypothesis as a means to explain other phenomena such as mid-plate swells (Detrick & Crough 1978), it is not required to explain the subsidence of drowned volcanic islands. Indeed, a combination of a load-induced stress relaxation and thermal contraction of the underlying lithosphere appears to be all that might be necessary in order to explain the subsidence history of atolls and their submerged counterparts, the guyots.

5.3 Stratigraphy of the flexural moats that flank oceanic islands

The subsidence and uplift history of oceanic islands is manifest not only in tide-gauge, archaeological, and coral reef data, but also in the stratigraphy of the flexural moats that flank them. There is now good sonar evidence (Moore *et al.* 1989), for example, that the flanks of oceanic islands and seamounts are subject to large-scale slope failures. The material involved in these failures moves downslope and into the flanking moats. If the moat geometry changes with time, as our multilayered viscoelastic plate model predicts (e.g. Fig. 12), their stratigraphic 'architecture' maybe a 'tape-recorder' of these changes.

Fig. 15 shows the stratigraphic implications of the multilayered viscoelastic plate model. Two models have been constructed. In both models, it has been assumed that during a particular stress relaxation 'event' sedimentary material has been able to infill the flexural moat up to a horizontal surface. In Fig. 15(a), it is assumed that the moat geometry is given by the deformation at the base of the flexed oceanic crust (i.e. the Moho), whereas in Figs 15(b) and (c) it follows that of the surface topography. The only difference between Figs 15(b) and (c) concerns whether the top of the subsiding load also accumulates sediments at the same time as the moat fills.

The main result shown in Fig. 15 is that the multilayered model predicts a pattern of offlap which represents the stratigraphic response to the decreasing width of the moat as stresses in the underlying lithosphere relax. Within each offlap 'sequence', we see onlap which reflects the gradual filling up of the moat. This is illustrated in Figs 15(b) and (c), which show the geometry of three once-flat stratigraphic horizons in the moat that formed in the period 10–100 kyr.

The predicted patterns of offlap and onlap in the flexural moats are in general agreement with observations. For example, ten Brink & Watts (1985) and Rees *et al.* (1993) have used seismic

Figure 15. Predicted stratigraphy of the flexural moats that flank seamounts and oceanic islands based on a multilayered viscoelastic plate model. The stratigraphy has been computed for six time steps. During each step, the moat geometry has been computed using a multilayered viscoelastic model with $E=120$ KJ mol^{-1} and a reference viscosity of 10^{20} Pa s, and sediments are assumed to fill the moat up to a horizontal surface. (a) Moat geometry given by the flexure at the base of the oceanic crust (i.e. Moho). (b) Moat geometry given by the top of the oceanic crust which includes the volcanic load. (c) As (b), except that sediments are assumed to accumulate on the crest of the load also.

reflection profiles to characterize the stratigraphic patterns that occur in the Hawaiian moat. They show that on cross-moat profiles the moat is characterized by a lowermost unit that onlaps the flexural bulge, a middle offlapping unit that migrates back towards the islands, and an uppermost ponded unit in the deepest part of the moat. They attribute the offlap pattern to variations in the flux of sedimentary material into the moat, due, for example, to the fact that individual islands in the chain are subject to large-scale flank collapses at different times. Rees *et al.* (1993) also examined the patterns on along-moat profiles. They showed that patterns of offlap and onlap are also seen in along-moat profiles. They attributed these patterns to progressive loading of an elastic plate by successive volcanoes in the chain.

While we concur with Rees *et al.* (1993) that offlap and onlap patterns on along-moat profiles are due to progressive loading of what is essentially an elastic plate, we disagree with their interpretation of the offlap patterns on the cross-moat profiles. The models in Fig. 15 suggest that variations in material flux, say from nearby islands, are not the only means of explaining offlap patterns that develop in flexural moats. The offlap could be the consequence of a reduction in the width of the moat due to stress relaxation in the underlying lithosphere. Unfortunately, the stratigraphic infill in flexural moats has been dated in only a few localities so it is not yet possible using current data sets to test this hypothesis fully.

6 CONCLUSIONS

We can draw the following conclusions from this study.

(1) The elastic thickness of the oceanic lithosphere, T_e, is, as suggested by previous studies, a function of the thermal age of the lithosphere at the time of loading, being well described by the depth to the 300–600 °C oceanic isotherms, based on plate-cooling models.

(2) There is evidence (e.g. Figs 2 and 3) that, for a particular thermal age, oceanic T_e decreases with age following loading. The decrease is most rapid during the first 1–2 Myr after loading, but appears to continue on longer timescales, although changes during 1–2 to 100 Myr are small.

(3) The dependence of T_e on thermal and load age can be explained by a model in which it is assumed that the lithosphere responds to surface loading in a manner similar to that in which a multilayered viscoelastic plate would. The model is based on the results of laboratory studies which suggest that creep is a thermally activated process, and observations of depth of the seafloor which suggest that the thermal structure of the lithosphere is given by the plate-cooling model.

(4) Comparisons of the predictions of two-layer multilayered viscoelastic models with the more widely used thin viscoelastic and elastic plate models show them to be special 'end-member' cases. The widespread success of the elastic plate model is attributed to the fact that the uppermost part of the oceanic lithosphere has such a high viscosity that it behaves, in effect, as an elastic plate on long timescales.

(5) The flexural rigidity at seamounts and oceanic islands that formed on >80 Ma old lithosphere can be explained by a multilayered viscoelastic model with a reference viscosity of 10^{20} Pa s and an activation energy of 120 KJ mol^{-1}. A higher activation energy would require a lower viscosity, while a lower activation energy would require a higher viscosity. If we assume a reference viscosity of 10^{20} Pa s, then the oceanic lithosphere appears to be associated with a significantly smaller activation energy than is indicated from experimental studies of diffusion and dislocation creep.

(6) A multilayered viscoelastic model explains the pattern of subsidence and uplift that followed the submarine phase of volcanism on Hawaii at 0.5 Ma. In particular, the model explains the fact that first Oahu and then Lanai experienced uplift at the time that Hawaii was sinking. More difficult to explain by the model is the detailed subsidence history of Hawaii, probably because of uncertainties in the island's loading history.

(7) A multilayered viscoelastic model explains the rapid subsidence of atolls, as indicated in the thickness of their fringing reefs, and does not require that the lithosphere beneath them was excessively heated and thinned at the time of loading.

(8) A multilayered viscoelastic model can also explain the stratigraphic patterns that develop in the flexural moats that flank oceanic islands. In particular, the model predicts patterns of offlap which reflect the stress relaxation and onlap as the moats are infilled by flat-lying material.

(9) Although the oceanic lithosphere is characterized by a long-term stress relaxation, it is not significant enough to prevent the use of T_e estimates to deduce the provenance of seamounts and oceanic islands. To the contrary, there seems to be a certain 'permanence' to the observations of flexure which enables the tectonic setting of a bathymetric feature on the ocean floor to be inferred directly from its T_e structure.

ACKNOWLEDGMENTS

This work was completed while ABW was a Crosby Visiting Professor at MIT. We acknowledge the support of a NERC ROPA grant to ABW. SZ acknowledges the support of a NASA grant to Dr Maria Zuber. Figs 1–10 were constructed using GMT software (Wessel & Smith 1991).

REFERENCES

Apple, R.A. & Macdonald, G.A., 1966. The rise of sea level in contemporary times at Honaunau, Hawaii, *Pacific Sci.,* **20,** 125–136.

Bodine, J.H., Steckler, M.S. & Watts, A.B., 1981. Observations of flexure and the rheology of the oceanic lithosphere, *J. geophys. Res.,* **86,** 3695–3707.

Bowin, C. & Milligan, J., 1985. Negative gravity anomaly over spreading rift valleys: Mid-Atlantic ridge at 26°N, *Tectonophysics,* **113,** 233–256.

Byerlee, J.D., 1978. Friction of rocks, *Pageoph,* **116,** 615–626.

Caldwell, J.G., Haxby, W.F., Karig, D.E. & Turcotte, D.L., 1976. On the applicability of a universal elastic trench profile, *Earth planet. Sci. Lett.,* **31,** 239–246.

Caldwell, J.G. & Turcotte, D.L., 1979. Dependence of the elastic thickness of the oceanic lithosphere on age, *J. geophys. Res.,* **84,** 7572–7576.

Calmant, S., 1987. The elastic thickness of the lithosphere in the Pacific Ocean, *Earth planet. Sci. Lett.,* **85,** 277–288.

Calmant, S. & Cazenave, A., 1986. The effective elastic lithosphere under the Cook-Austral and Society islands, *Earth planet. Sci. Lett.,* **77,** 187–202.

Calmant, S., Francheteau, J. & Cazenave, A., 1990. Elastic layer thickening with age of the oceanic lithosphere, *Geophys. J.,* **100,** 59–67.

Cathles, L.M., 1975. *The Viscosity of the Earth's Mantle,* Princeton University Press, Princeton.

Cazenave, A. & Dominh, K., 1984. Geoid heights over the Louisville Ridge (South Pacific), *J. geophys. Res.,* **89,** 11 171–11 179.

Cazenave, A., Lago, B., Dominh, K. & Lambeck, K., 1980. On the response of the ocean lithosphere to seamount loads from Geos 3 satellite radar altimeter observations, *Geophys. J. R. astr. Soc.,* **63,** 233–252.

Clague, D.A. & Jarrard, R.D., 1973. Tertiary Pacific Plate motion deduced from the Hawaiian–Emperor Chain, *Geol. Soc. Am. Bull.,* **84,** 1135–1154.

Cloetingh, S. & Burov, E.B., 1996. Thermomechanical structure of European continental lithosphere: constraints from rheological profiles and EET estimates, *Geophys. J. Int.,* **124,** 695–723.

Cochran, J.R., 1973. Gravity and magnetic investigations in the Guiana Basin, Western Equatorial Atlantic, *Geol. Soc. Am. Bull.,* **84,** 3249–3268.

Cochran, J.R., 1979. An analysis of isostasy in the world's oceans 2. Midocean ridge crests, *J. geophys. Res.,* **84,** 4713–4729.

Courtney, R.C. & Beaumont, C., 1983. Thermally-activated creep and flexure of the oceanic lithosphere, *Nature,* **305,** 201–204.

Dañobeitia, J.J. & Canales, J.P., 1994. An estimation of the elastic thickness of the lithosphere in the Canary archipelago using admittance function, *Geophys. Res. Lett.,* **21,** 2649–2652.

Dañobeitia, J.J., Canales, J.P. & Dehghani, G.A., 1994. An estimation of the elastic thickness of the lithosphere in the Canary Archipelago using admittance function, *Geophys. Res. Lett.,* **21,** 2649–2652.

Detrick, R.S. & Crough, S.T., 1978. Island subsidence, hot spots, and lithospheric thinning, *J. geophys. Res.,* **83,** 1236–1244.

Detrick, R.S. & Watts, A.B., 1979. An analysis of isostasy in the world's oceans, 3. Aseismic Ridges, *J. geophys. Res.,* **84,** 3637–3653.

Feighner, M.A. & Richards, M.A., 1994. Lithospheric structure and compensation mechanism of the Galapogos Arc, *J. geophys. Res.,* **99,** 6711–6729.

Filmer, P.E. & McNutt, M.K., 1989. Geoid Anomalies over the Canary Islands Group, *Mar. geophys. Res.,* **11,** 77–87.

Fischer, K.M., McNutt, M.K. & Shure, L., 1986. Thermal and mechanical constraints on the lithosphere beneath the Marquesas swell, *Nature,* **332,** 733–736.

Fjeldskaar, W., 1994. Viscosity and thickness of the asthenosphere detected from Fennoscandian uplift, *Earth planet. Sci. Lett.,* **126,** 399–410.

Goetze, C., 1978. The mechanisms of creep in olivine, *Phil. Trans. R. Soc. Lond.,* A**288,** 99–119.

Goodwillie, A.M. & Watts, A.B., 1993. An altimetric and bathymetric study of elastic thickness in the central Pacific ocean, *Earth. planet. Sci. Lett.,* **118,** 311–326.

Grigg, R.W. & Jones, A.T., 1997. Uplift caused by lithospheric flexure in the Hawaiian Archipelago as revealed by elevated coral deposits, *Mar. Geol.,* **141,** 11–25.

Gunn, R., 1943a. A quantitative evaluation of the influence of the lithosphere on the anomalies of gravity, *Franklin Inst. J.,* **236,** 47–65.

Harris, R.N. & Chapman, D.S., 1994. A comparison of mechanical thickness estimates from trough and seamount loading in the southeastern Gulf of Alaska, *J. geophys. Res.,* **99,** 9297–9317.

Hirth, G. & Kohlstedt, D.L., 1996. Water in the oceanic upper mantle: implications for rheology, melt extraction and the evolution of the lithosphere, *Earth planet. Sci. Lett.,* **144,** 93–108.

Ito, G., McNutt, M.K. & Gibson, R.L., 1995. Crustal structure of the Tuamotu Plateau, 15°S, and implications for its origin, *J. geophys. Res.,* **100,** 8097–8114.

Iwasaki, T. & Matsu'ura, M., 1982. Quasi-static crustal deformations due to a surface load: rehological structure of the Earth's crust and upper mantle, *J. Phys. Earth,* **30,** 469–508.

Judge, A.V. & McNutt, M.K., 1991. The relationship between plate curvature and elastic plate thickness: a study of the Peru–Chile trench, *J. geophys. Res.,* **96,** 16 625–16 640.

Karato, S. & Wu, P., 1993. Rheology of the Upper Mantle, *Science,* **260,** 771–778.

Karner, G.D., 1982. Spectral representation of isostatic models, *BMR J. Aust. Geol. Geophys.,* **7,** 55–62.

Karner, G.D. & Weissel, J.K., 1990. Factors controlling the location of compressional deformation of oceanic lithosphere in the Central Indian ocean, *J. geophys. Res.,* **95,** 19 795–19 810.

Kruse, S.E., Liu, Z.J., Naar, D.F. & Duncan, R.A., 1997. Effective elastic thickness of the lithosphere along the Easter Seamount Chain, *J. geophys. Res.,* **102,** 27305–27 317.

Kuo, B.Y. & Parmentier, E.M., 1986. Flexure and thickening of the lithosphere at the East Pacific Rise, *Geophys. Res. Lett.,* **13,** 681–684.

Lambeck, K., 1981a. Flexure of the ocean lithosphere from island uplift, bathymetry and geoid height observations: the Society Islands, *Geophys. J. R. astr. Soc.,* **67,** 91–114.

Lambeck, K., 1981b. Lithospheric response to volcanic loading in the Southern Cook Islands, *Earth planet. Sci. Lett.,* **55,** 482–496.

Lambeck, K. & Nakiboglu, S.M., 1981. Seamount loading and stress in the ocean lithosphere 2. Viscoelastic and elastic-viscoelastic models, *J. geophys. Res.,* **86,** 6961–6984.

Levitt, D.A. & Sandwell, D.T., 1995. Lithospheric bending at subduction zones based on depth soundings and satellite gravity, *J. geophys. Res.,* **100,** 379–400.

Ludwig, K.R., Szabo, B.J., Moore, J.G. & Simmons, K.R., 1991. Crustal subsidence rate of Hawaii determined from $^{234}U/^{238}U$ ages of drowned coral reefs, *Geology,* **19,** 171–174.

McAdoo, D.C. & Martin, C.F., 1984. Seasat observations of lithospheric flexure seaward of trenches, *J. geophys. Res.,* **89,** 3201–3210.

McAdoo, D.C., Caldwell, J.G. & Turcotte, D.L., 1978. On the elastic–perfectly plastic bending of the lithosphere under generalized loading with application to the Kuril Trench, *Geophys. J. Int.,* **54,** 11–26.

McAdoo, D., Martin, C.F. & Poulouse, S., 1985. Seasat observations of flexure: Evidence for a strong lithosphere, *Tectonophysics,* **116,** 209–222.

McConnell, R.K., 1968. Viscosity of the mantle from relaxation time spectra of isostatic adjustment, *J. geophys. Res.,* **73,** 7089–7105.

McKenzie, D.P. & Bowin, C.O., 1976. The relationship between bathymetry and gravity in the Atlantic Ocean, *J. geophys. Res.,* **81,** 1903–1915.

McNutt, M.K., 1979. Compensation of oceanic topography: an application of the response function technique to the Surveyor area, *J. geophys. Res.,* **84,** 7589–7598.

McNutt, M.K., 1984. Lithospheric flexure and thermal anomalies, *J. geophys. Res.,* **89,** 11 180–11 194.

McNutt, M.K., 1988. Thermal and mechanical properties of the Cape Verde Rise, *J. geophys. Res.,* **93,** 2784–2794.

McNutt, M.K. & Menard, H.W., 1978. Lithospheric flexure and uplifted atolls, *J. geophys. Res.,* **83,** 1206–1212.

McNutt, M.K. & Parker, R.L., 1978. Isostasy in Australia and the evolution of the compensation mechanism, *Science,* **199,** 773–775.

Madsen, J.A., Forsyth, D.W. & Detrick, R.S., 1984. A new isostatic model for the East Pacific Rise Crest, *J. geophys. Res.,* **89,** 9997–10 016.

Menard, H.W., 1983. Insular erosion, isostasy and subsidence, *Science,* **220,** 913–917.

Minshull, T.A. & Brozena, J.M., 1997. Gravity anomalies and flexure of the lithosphere at Ascension Island, *Geophys. J. Int.,* **131,** 347–360.

Mitrovica, J.X. & Forte, A.M., 1997. Radial profile of mantle viscosity: Results from the joint inversion of convection and post-glacial rebound observables, *J. geophys. Res.,* **102,** 2751–2769.

Mitrovica, J.X. & Peltier, W.R., 1993. The inference of mantle viscosity from the inversion of the Fennoscandian relaxation spectrum, *Geophys. J. Int.,* **114,** 45–62.

Moore, J.G., 1970. Relationship between subsidence and volcanic load, Hawaii, *Bull. Volcanol.,* **34,** 562–576.

Moore, J.G. & Campbell, J.F., 1987. Age of tilted reefs, Hawaii, *J. geophys. Res.,* **92,** 2641–2646.

Moore, J.M. & Fornari, D.J., 1984. Drowned reefs as indicators of the rate of subsidence of the island of Hawaii, *J. Geol.,* **92,** 752–759.

Moore, J.G., Clague, D.A., Holcomb, R.T., Lipman, P.W., Normark, W.R. & Torresan, M.E., 1989. Prodigous submarine landslides on the Hawaiian Ridge, *J. geophys. Res.,* **94,** 17 465–17 484.

Nadai, A., 1963. *Theory of Flow and Fracture of Solids*, Vol. 2, McGraw-Hill, New York.

Newman, R. & White, N., 1997. Rheology of the continental lithosphere inferred from sedimentary basins, *Nature,* **385,** 621–624.

Nishimura, C.E. & Forsyth, D.W., 1989. The anisotropic structure of the upper mantle in the Pacific, *Geophys. J.,* **96,** 203–229.

Parsons, B.E. & Sclater, J.G., 1977. An analysis of the variation of ocean floor bathymetry and heat flow with age, *J. geophys. Res.,* **82,** 803–827.

Quinlan, G.M. & Beaumont, C., 1984. Appalachian thrusting, lithospheric flexure and the Paleozoic stratigraphy of the eastern Interior of North America, *Can. J. Earth Sci.,* **21,** 973–996.

Rees, B.A., Detrick, R.S. & Coakley, B.J., 1993. Seismic stratigraphy of the Hawaiian flexural moat, *Geol. Soc. Am. Bull.,* **105,** 189–205.

Sheehan, A.F. & McNutt, M.K., 1989. Constraints on thermal and mechanical structure of the oceanic lithosphere at the Bermuda Rise from geoid height and depth anomalies, *Earth planet. Sci. Lett.,* **93,** 377–391.

Sleep, N.H., 1992. Hotspot volcanism and mantle plumes, *Ann. Rev. Earth planet. Sci.,* **20,** 19–43.

Sleep, N.H. & Snell, N.S., 1976. Thermal contraction and flexure of mid-continent and Atlantic marginal basins, *Geophys. J. R. astr. Soc.,* **45,** 125–154.

Smith, W.H.F., Staudigel, H., Watts, A.B. & Pringle, M.S., 1989. The Magellan Seamounts: Early Cretaceous record of the South Pacific isotopic and thermal anomaly, *J. geophys. Res.,* **94,** 10 501–10 523.

Suyenaga, W., 1977. Earth deformation in response to surface loading: application to the formation of the Hawaiian Ridge, *PhD thesis,* University of Hawaii, Hawaii.

ten Brink, U.S. & Watts, A.B., 1985. Seismic stratigraphy of the flexural moat flanking the Hawaiian Islands, *Nature,* **317,** 421–424.

Vermeersen, L.L.A., Sabadini, R., Devoti, R., Luceri, V., Rutigliano, P., Sciarretta, C. & Bianco, G., 1998. Mantle viscosity inferences from joint inversions of Pleistocene deglaciation-induced changes in geopotential with a new SLR analysis and polar wander, *Geophys. Res. Lett.,* **25,** 4261–4264.

Walcott, R.I., 1970a. Flexural rigidity, and viscosity of the lithosphere, *J. geophys. Res.,* **75,** 3941–3953.

Walcott, R.I., 1970b. Flexure of the lithosphere at Hawaii, *Tectonophysics,* **9,** 435–446.

Walcott, R.I., 1970c. Isostatic response to loading of the crust in Canada, *Can. J. Earth Sci.,* **7,** 716–727.

Wang, X. & Cochran, J.R., 1993. Gravity anomalies, isostasy and mantle flow at the East Pacific Rise crest, *J. geophys. Res.,* **98,** 19 505–19 531.

Watts, A.B., 1978. An analysis of isostasy in the world's oceans: 1. Hawaiian–Emperor seamount chain, *J. geophys. Res.,* **83,** 5989–6004.

Watts, A.B., 1994. Crustal structure, gravity anomalies and flexure of the lithosphere in the Canary Islands, *Geophys. J. Int.,* **119,** 648–666.

Watts, A.B. & Cochran, J.R., 1974. Gravity anomalies and flexure of the lithosphere along the Hawaiian–Emperor seamount chain, *Geophys. J. R. astr. Soc.,* **38,** 119–141.

Watts, A.B. & Ribe, N.M., 1984. On geoid heights and flexure of the lithosphere at seamounts, *J. geophys Res.,* **89,** 11 152–11 170.

Watts, A.B. & ten Brink, U.S., 1989. Crustal structure, flexure and subsidence history of the Hawaiian Islands, *J. geophys. Res.,* **94,** 10473–10 500.

Watts, A.B., Cochran, J.R. & Selzer, G., 1975. Gravity anomalies and flexure of the lithosphere: a three-dimensional study of the Great Meteor Seamount, N.E. Atlantic, *J. geophys. Res.,* **80,** 1391–1398.

Watts, A.B., Bodine, J.H. & Ribe, N.M., 1980. Observations of flexure and the geological evolution of the Pacific Ocean basin, *Nature,* **283,** 532–537.

Watts, A.B., Peirce, C., Collier, J., Dalwood, R., Canales, J.P. & Henstock, T.J., 1997. A seismic study of lithospheric flexure in the vicinity of Tenerife, Canary Islands, *Earth planet. Sci. Lett.,* **146,** 431–447.

Wessel, P., 1993. A re-examination of the flexural deformation beneath the Hawaiian Islands, *J. geophys. Res.,* **98,** 12 177–12 190.

Wessel, P. & Haxby, W.F., 1990. Thermal stresses, differential subsidence, and flexure at oceanic fracture zones, *J. geophys. Res.,* **95,** 375–391.

Wessel, P. & Smith, W.H.F., 1991. Free software helps map and display data, *EOS, Trans. Am. geophys. Un.,* **72,** 441–446.

Wolf, D., 1987. An upper bound on lithosphere thickness from glacioisostatic adjustment in Fennoscandia, *J. Geophys.,* **61,** 141–149.

Wu, P. & Peltier, W.R., 1983. Glacial isostatic adjustment and the free-air gravity anomaly as a constraint on deep mantle viscosity, *Geophys. J. R. astr. Soc.,* **74,** 377–449.

Zhong, S., 1997. Dynamics of crustal compensation and its influences on crustal isostasy, *J. geophys. Res.,* **102,** 15 287–15299.